Attribution of climate change and human activities to streamflow variations with a posterior distribution of hydrological simulations

Xiongpeng Tang [1, 2, 3], Guobin Fu [4], Silong Zhang [1], Chao Gao [1], Guoqing Wang [2, 3], Zhenxin Bao [2, 3], Yanli Liu [2, 3], Cuishan Liu [2, 3], Junliang Jin [2, 3]

5   [1]Guangdong-Hong Kong Joint Laboratory for Water Security, Beijing Normal University at Zhuhai, Zhuhai, 519087, China

[2]State Key Laboratory of Hydrology-Water Resources and Hydraulic Engineering, Nanjing 210098, China

[3]Nanjing Hydraulic Research Institute, Nanjing 210029, China

[4] CSIRO, Land and Water, Private Bag 5, Wembley, WA 6913, Australia

Correspondence to: Guoqing Wang (gqwang@nhri.com)

10   **Abstract:** Hydrological simulations are a main method of quantifying the contribution rate (CR) of climate change (CC) and human activities (HAs) to watershed streamflow changes. However, the uncertainty of hydrological simulations is rarely considered in current research. To fill this research gap, based on the Soil and Water Assessment Tool (SWAT) model, in this study, we propose a new framework to quantify the CR of CC and HAs based on the posterior histogram distribution of hydrological simulations. In our new quantitative framework, the uncertainty of hydrological simulations is first considered to

15   quantify the impact of "equifinality for different parameters", which is common in hydrological simulations. The Lancang River (LR) Basin in China, which has been greatly affected by HAs in the past two decades, is then selected as the study area. The global gridded monthly sectoral water use data set (GMSWU), coupled with the dead capacity data of the large reservoirs within the LR basin and the Budyko hypothesis framework, are used to compare the calculation result of the novel framework. The results show that (1) the annual streamflow at Yunjinghong station in the Lancang River Basin changed abruptly in 2005, which was mainly

20   due to the construction of the Xiaowan hydropower station that started in October 2004. The annual streamflow and annual mean temperature time series from 1961 to 2015 in the LR Basin showed a significant decreasing and increasing trend at the $\alpha = 0.01$ significance level, respectively. The annual precipitation showed an insignificant decreasing trend. (2) The results of quantitative analysis using the new framework showed that the reason for the decrease in the streamflow at Yunjinghong station was 42.6% due to CC, and the remaining 57.4% was due to HAs, such as the construction of hydropower stations within the study area. (3)

25   The comparison with the other two methods showed that the CR of CC calculated by the Budyko framework and the GMSWU data were 37.2% and 42.5%, respectively, and the errors of the calculations of the new framework proposed in this study were within 5%. Therefore, the newly proposed framework, which considers the uncertainty of hydrological simulations, can accurately quantify the CR of CC and HAs to streamflow changes. (4) The quantitative results calculated by using the simulation results with the largest Nash-Sutcliffe efficiency coefficient (NSE) indicated that CC was the dominant factor for streamflow reduction, which

30   was in opposition to the calculation results of our new framework. In other words, our novel framework could effectively solve the calculation errors caused by the "equifinality for different parameters" of hydrological simulations. (5) The results of this case study also showed that the reduction in the streamflow in June and November was mainly caused by decreased precipitation and increased evapotranspiration, while the changes in the streamflow in other months were mainly due to HAs such as the regulation of the constructed reservoirs. In general, the novel quantitative framework that considers the uncertainty of hydrological

35   simulations presented in this study has validated an efficient alternative for quantifying the CR of CC and HAs to streamflow changes.

Key words: Attribution analysis; Climate change; Human activities; Lancang River Basin; Uncertainty; SWAT model

1. Introduction

Both the hydrological cycle of the watershed and water resource systems are deeply influenced by climate change (CC) and
40   human activities (HAs) (Bao et al., 2012; Chandesris et al., 2019; Han et al., 2019; Teuling et al., 2019). CC mainly refers to changes in precipitation and evapotranspiration that are caused by rising temperatures and water vapor (Hegerl et al., 2015), while the impact of HAs is mainly reflected in the following aspects: reservoir construction changes the spatial and temporal distribution of streamflow processes (Hennig et al., 2013; Chandesris et al., 2019); land use changes change the characteristics of the underlying surface of the watershed, in turn affecting the streamflow of the watershed (Yang et al., 2017); population increase
45   leads to an increase in the amount of water used for domestic consumption (Teuling et al., 2019), etc. However, identifying which CC and HAs are the main factors driving the changes in the water cycle of river basins is of great significance for water resource managers to formulate policies for sustainable water resource utilization (Dey and Mishra, 2017; Liu et al., 2017). If CC is the dominant driving factor, then hydro-meteorologists need to assess the future trends of meteorological factors, such as precipitation and temperature, to change their water resource management strategies in a timely manner. Conversely, if HAs are the dominant
50   factor, water resource managers should evaluate whether the impact of these HAs exceeds the local water resource carrying capacity and then adjust their related policies (Fu et al., 2004).

Numerous published articles have focused on how to quantify the CR of CC and HAs to the streamflow change in river basins (Liu et al., 2019; Bao et al., 2012; Chandesris et al., 2019; Han et al., 2019; Kong et al., 2016; Xie et al., 2019). In general, the commonly used methods of attribution analysis can be divided into the following three categories: 1) conceptual methods, such
55   as the Budyko framework (Li et al., 2007; Liu et al., 2017); 2) hydrological simulation methods (Liu et al., 2019); and 3) analytical methods, such as the climate elasticity method (Liang et al., 2013). What these three methods have in common is that they all need to first test the annual streamflow sequence through non-stationary testing methods (such as the Mann-Kendall test), and then divide the study period into the natural period (before the break point) and the impacted period (after the break point). The first type of method needs to first calculate the sensitivity of the basin's precipitation and potential evapotranspiration to
60   hydrological variables, and then the hydrological changes caused by CC can be calculated combined with the hydrological sensitivity parameters through the changes in precipitation and potential evapotranspiration in the impacted period and natural period so that the CR of HAs is obtained based on the water balance equation (Li et al., 2007). The second type of method simulates multiple scenarios by changing one impact factor with other fixed factors to evaluate the CR of the changed factor using lumped or distributed hydrological models (Liu et al., 2019). The core of these methods is the modelling of two situations where only one
65   impact factor state has been changed, and the difference between the two simulation results is regarded as the influence of the changed factor. The third type of method is mostly based on numerical calculation, taking the climate elasticity method as an example (Liang et al., 2013), this method introduces the concept of climate elasticity to define the quantitative relationship between changes in streamflow and climatic variables (precipitation, evapotranspiration, etc.), and the CR of HAs to streamflow changes can be obtained by subtracting the CR of climate variables. Among the three types of methods, the second type methods are the
70   most widely used because it has the following advantages: 1) relatively small data requirements (one only needs to input the

meteorological and hydrological data to the hydrological model); 2) relatively simple theoretical assumptions; and 3) can quantify the CR of CC and HAs to streamflow changes at the monthly scale.

Various related published articles are briefly reviewed as follows. Bao et al. (2012) used the variable infiltration capacity (VIC) model to investigate the impacts of CC and HAs on streamflow changes in the Haihe River Basin, China, and they concluded that HA accounted for more than 70% of the decrease in streamflow at Guantai station. Wang et al. (2013) used a two-parameter hydrological model to quantify the contribution of CC and HAs to streamflow changes in three river basins (i.e., Zhanghe, Chaohe, and Hutuo River), and they found that HAs were the dominant factor in streamflow changes. The above literature review shows that these studies all used hydrological simulations with fixed parameter sets to quantify the impact of CC and HAs. As pointed out by Abbaspour et al. (2004) and Zhao et al. (2018a), there is a phenomenon of "equifinality for different parameters" (Beven, 2006) in hydrological calibration and simulation, which also means that we cannot ignore the uncertainty of model parameters in the process of quantifying the CR of CC and HAs to streamflow changes because two sets of parameters with the same performance (with the same Nash-Sutcliffe efficiency coefficient) may lead to very different results; this will further influence the decision-making of water resource managers to make effective and sustainable water resource utilization policies. In the last few decades, great progress has been made in evaluating the uncertainty of hydrological simulations (Abbaspour et al., 2004; Beven and Binley, 1992; Yang et al., 2008; Zhao et al., 2018a; Farsi and Mahjouri, 2019); however, in studies related to quantifying the CR of CC and HAs for streamflow changes, few studies have considered the uncertainty of hydrological simulations (Farsi and Mahjouri, 2019). According to our literature search, Farsi and Mahjouri (2019) first considered the uncertainty of hydrological simulations in the process of quantifying the CR of CC and HAs to streamflow changes, but they only constructed the posterior distribution of the CRs of CC and HAs; in their research, they did not specify how to calculate the CRs of CC and HAs while considering the uncertainty of hydrological simulations. Therefore, to fill this research gap, in this study we propose a new method to quantify the contribution of CC and HAs to streamflow changes considering the uncertainty of hydrological simulations, which in summary, is developed using the posterior histogram distribution of hydrological simulations.

The Lancang River (LR) is located in southwest China, and is the largest transboundary river in the Indo-China Peninsula; it is usually called the Mekong River (MR) after flowing out of China (Grumbine and Xu, 2011). The abundant water and ecological diversity of the Lancang-Mekong River Basin nurtures tens of millions of people in many countries along the Lancang-Mekong River. The upstream flow of the river provides guarantees for irrigation and fishery water use in the countries along the MR during the dry season, and the water conservancy facilities of the LR during the peak of the flood period also provide important engineering guarantees for downstream flood control (Piman et al., 2012; Piman et al., 2016). In the past three decades, a series of hydropower stations have been constructed in the LR Basin to meet the flood control and drought relief requirements of downstream countries and the power needs of Southwest China. Therefore, it is particularly important to quantify the CR of CC and HAs to streamflow changes in the LR Basin. However, so far, there are still few corresponding studies. Han et al. (2019) chose the LR Basin as the study area and then divided the research period into three periods, the natural period, transition period, and impacted period, and combined them with the construction time of six large hydropower stations in the LR area. Finally, they found that the CR of HAs during the impact period exceeded 95%, using the coupled routing and excess storage (CREST) model, which was probably due to the construction of the Nuozhadu hydropower station. However, there are still areas for improvement in their research: 1) the results of the hydrological simulation were relatively poor (with monthly NSE = 0.57 for the whole study period), and 2) the uncertainty involved in hydrological simulations was not considered.

In this paper, the breakpoint of the change in flow regimes was identified using the Mann-Kendall break point test. Then, the study period was divided into a natural period (before the breakpoint) and an impacted period (after the breakpoint). The Soil and Water Assessment Tool (SWAT) model was used for monthly streamflow simulation at the Yunjinghong station. Next, the monthly SWAT model was calibrated and validated using the sequential uncertainty fitting procedure version 2 (SUFI-2) (Abbaspour et al., 2004). Uncertainty analysis was also conducted with the SUFI-2 method, and then the posterior histogram frequency distribution (HFD) of the CR of CC and HAs was obtained. Finally, the proposed quantification framework was compared with two other methods: one was the Budyko framework, and the other was to use the LR Basin's gridded monthly sectoral water withdrawals in the period from 1971 to 2010 (Huang et al., 2018) together with the dead reservoir storage capacity data of the six constructed hydropower stations along the main stream of LR, to separate the CR of HAs.

2. Study area and data sets

2.1 Study area

The Lancang River (LR) originates in the northeastern Tanggula Mountains, Qinghai Province, China, and flows through China's Qinghai Province, Tibet Autonomous Region and Yunnan Province. It is the largest international river in Southeast Asia, and it is called the Mekong River after it flows out of China. Its main stream has a total length of ~2161 km and a total catchment area of ~160000 km^2 (Han et al., 2019; Li et al., 2017a). The topography of the LR is characterized by high northern and low southern portions; the maximum elevation in the northern mountainous area can reach ~5871 meters, while the lowest elevation in the downstream area is only ~547 meters (Fig. 1). This steep terrain difference also leads to the LR having a large potential for hydropower resources. During the past few decades, Huaneng Lancangjiang Hydropower Co., Ltd. constructed six large hydropower stations (i.e., Gongguoqiao, Xiaowan, Manwan, Dachaoshan, Nuozhadu and Jinghong) on the main stream of the LR to meet the demands for power and irrigation water in Southwest China (Fig. 1 and Table 1) (Han et al., 2019; Hennig et al., 2013; Xue et al., 2011). At the same time, the construction of these hydropower stations has greatly reduced the risk of flooding in downstream countries and brought great convenience to using water for downstream agricultural irrigation. Detailed information on the six constructed hydropower stations is outlined in Table 1. These data are mainly collected from https://opendevelopmentmekong.net/topics/hydropower/, as well as from other published related literature (Han et al., 2019; Xue et al., 2011; Hennig et al., 2013; Tilt and Gerkey, 2016).

The LR features an arid climate in the upper mountainous areas, while the lower reaches are dominated by humid climates. The average annual precipitation of the whole basin is ~ 870 mm based on a 55-year record (from 1961 to 2015) using the China Gauge-based Daily Precipitation Analysis (CGDPA) (Xie et al., 2007; Tang et al., 2019). Due to the influence of the westerlies and the Indian Ocean monsoon, the precipitation in the LR has obvious seasonal changes, and the precipitation from June to September accounts for more than 70% of the annual precipitation (Jacobs, 2002). Correspondingly, the streamflow of the LR also shows seasonality, and the floods are mostly concentrated from June to September.
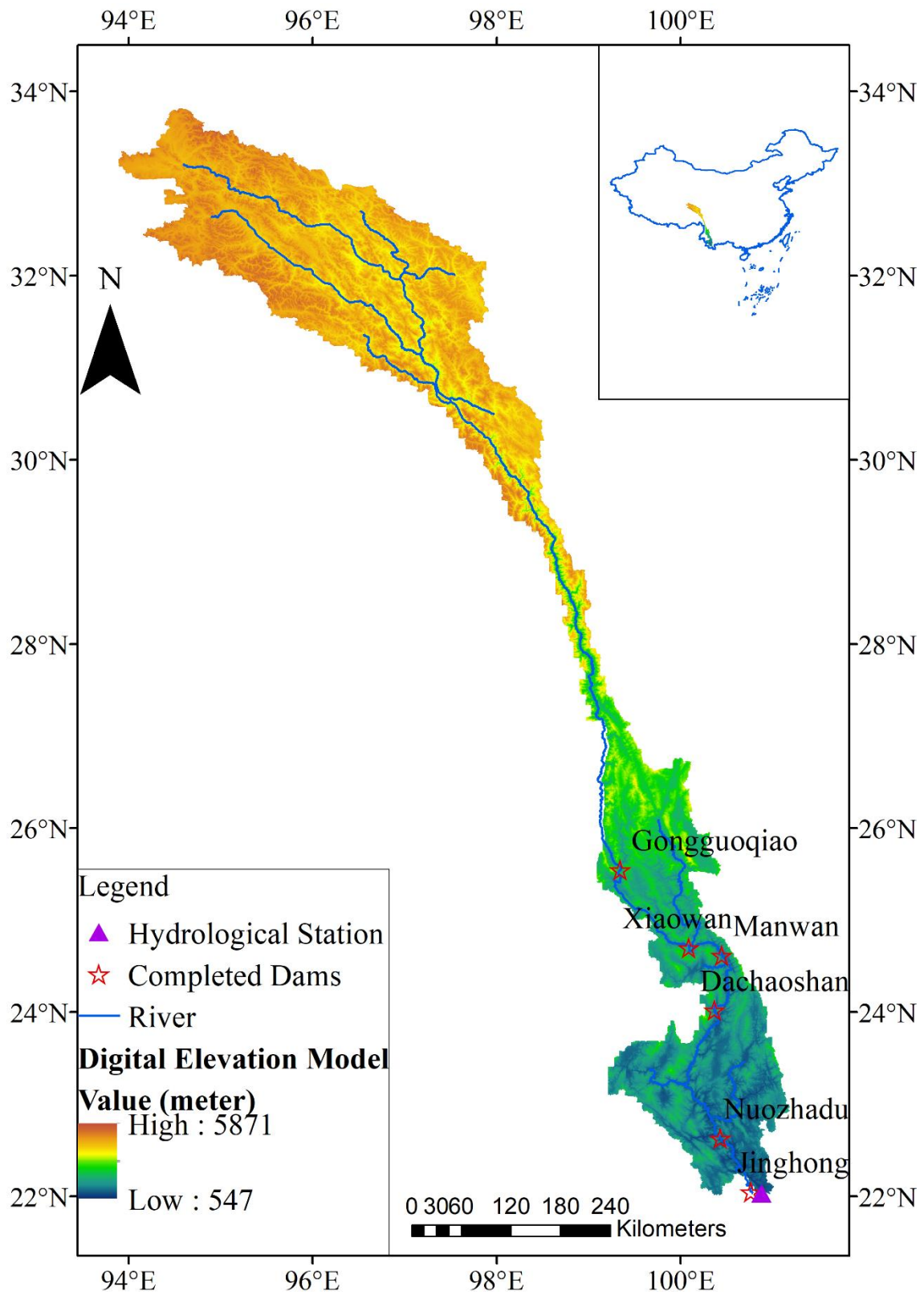
Fig. 1. Locations of the Lancang River (LR) Basin, Yunjinghong hydrological station, constructed dams on the main stream of the LRB, and main rivers and elevations (m).

Table 1 Basic information for the six large constructed dams on the mainstream of the LR Basin

Hydropower station	Manwan	Dachaoshan	Jinghong	Xiaowan	Gongguoqiao	Nuozhadu
Date of river closure	1987.12	1997.11	2005.01	2004.10	2008.12	2007.11
Date of complete construction	1995.06	2003.10	2009.05	2010.08	2012.03	2014.06
Drainage area (10^4 km^2)	11.45	12.10	14.91	11.33	9.73	14.47
Dead reservoir storage (km^3)	0.668	0.371	0.81	4.35	0.316	10.3
Total reservoir storage (km^3)	0.92	0.94	1.40	15.3	0.365	22.7
Installed capacity (10^4 kw)	150	135	150	420	90	500

145   (Notation: Dead storage capacity refers to the storage capacity below the dead water level of the reservoir, which does not participate in runoff regulation during the normal operation of the reservoir.)

2.2 Data sets

The China Gauge-based Daily Precipitation Analysis (CGDPA) product was developed by the China Meteorological Administration (CMA) using data from ~2400 ground-based national weather stations across China (Tang et al., 2018; Xie et al.,

150   2007; Shen et al., 2014). It provides daily precipitation, maximum temperature, minimum temperature, relative humidity, and wind speed data at a 0.25-degree spatial resolution from 1961 to 2015 (http://cdc.nmic.cn). Previous studies have successfully applied this product to multiple research areas in China (Tang et al., 2019; Tang et al., 2018; Han et al., 2019). The daily streamflow data from Yunjinghong station for the time period from 1961 to 2015 were collected from the Information Center of the Ministry of Water Resources and the local water resources management department.

155   The digital elevation model (DEM) used in this study was downloaded from NASA's Shuttle Radar Topography Mission (SRTM) data bank at a spatial resolution of ~90 meters (http://srtm.csi.cgiar.org/), which was used to generate the watershed boundary, slope and sub-watershed data in the SWAT model (Arnold et al., 2012a). The Harmonized World Soil Database (version 1.2) (HWSD v1.2) at a spatial resolution of ~1 km was downloaded from the Food and Agriculture Organization of the United Nations, and this data set contains two layers of soil. The land use and cover data with a spatial resolution of ~1km were collected

160   from the Geospatial Data Cloud (http://www.gscloud.cn/). In this study, to analyze the land use change in the LR during the historical period, we collected five periods of land use data in the 1980s, 1990s, 2000s, and from 2010 to 2015, and this data set was downloaded from the Geographic Information Monitoring Cloud Platform (http://www.dsac.cn/), with a spatial resolution of 30 meters.

The global gridded monthly sectoral water use (GMSWU) data set for 1971-2010 was obtained from

165   https://zenodo.org/record/1209296#.XsJmiTNlsSJ. This data set was developed by Huang et al. (2018), and it provides the global domestic water use, irrigation water use, livestock water use, manufacturing water use and mining water use with a spatial resolution of 0.5 degrees. This dataset is used in this study because it is difficult to collect water withdrawal data related to HAs in the LR Basin, and this dataset has been successfully applied in this basin in other studies (Han et al., 2019). And we used this data set here to roughly separate the effects of HAs in the LR. For more technical information about this set of products, the

170   readers can refer to Huang et al. (2018) and Han et al. (2019). Furthermore, detailed information on six large dams in the main stream of the LR was collected from Open Development Mekong (https://opendevelopmentmekong.net/topics/hydropower/) and

Huaneng Lancang River Hydropower Inc. It mainly includes the dates when the rivers start to be closed, when these dams were fully put into use, their dead storage capacity, their total storage capacity, and other information.

3. Methodologies

3.1 The novel proposed framework

Hydrological simulation is one of the main methodologies to quantify the CR of CC and HAs to streamflow variations; however, in the past, related studies have rarely considered the uncertainty involved in hydrological simulations (Farsi and Mahjouri, 2019). In this section, we will introduce a new quantitative framework to quantify the influence of the common phenomenon of "equifinality for different parameters" in hydrological simulation on the quantitative results, by constructing the posterior distribution of streamflow simulations during the implementation process. The specific implementation flowchart is shown in Fig. 2. The detailed execution steps are shown as follows.

Step 1: Inspection of break points in the annual streamflow sequence; based on the result of break point test, the entire time series is divided into a natural period (before the break point) and an impacted period (after the break point).

Step 2: Sensitivity analysis of the parameters in the hydrological model.

Step 3: According to the results of the parameter sensitivity analysis, selection of the more sensitive parameters and input of the hydrometeorological data of the natural period to calibrate the hydrological model with 1000 runs.

Step 4: Selection of the parameter sets with Nash-Sutcliffe efficiency coefficients (NSE) is greater than 0.75 in 1000 simulations, input of the hydrometeorological data of the impacted period, and further calculation of the CR of CC and HAs to the streamflow change corresponding to each simulation result.

Step 5: Construction of the posterior histogram distribution (PHD) of the CR of CC and HAs (with a 5% step), and then the histogram with the highest frequency is treated as the uncertainty CR interval of CC and HAs to the streamflow change.

Step 6: The arithmetic mean of the results in the interval is treated as its true CR.

In step 4, to ensure the number of streamflow simulation samples, we set the simulation results with NSE is greater than 0.75 to at least 500 times. If the setting is not met, then step 3 is repeated until the cumulative simulation times are greater than 500 times.
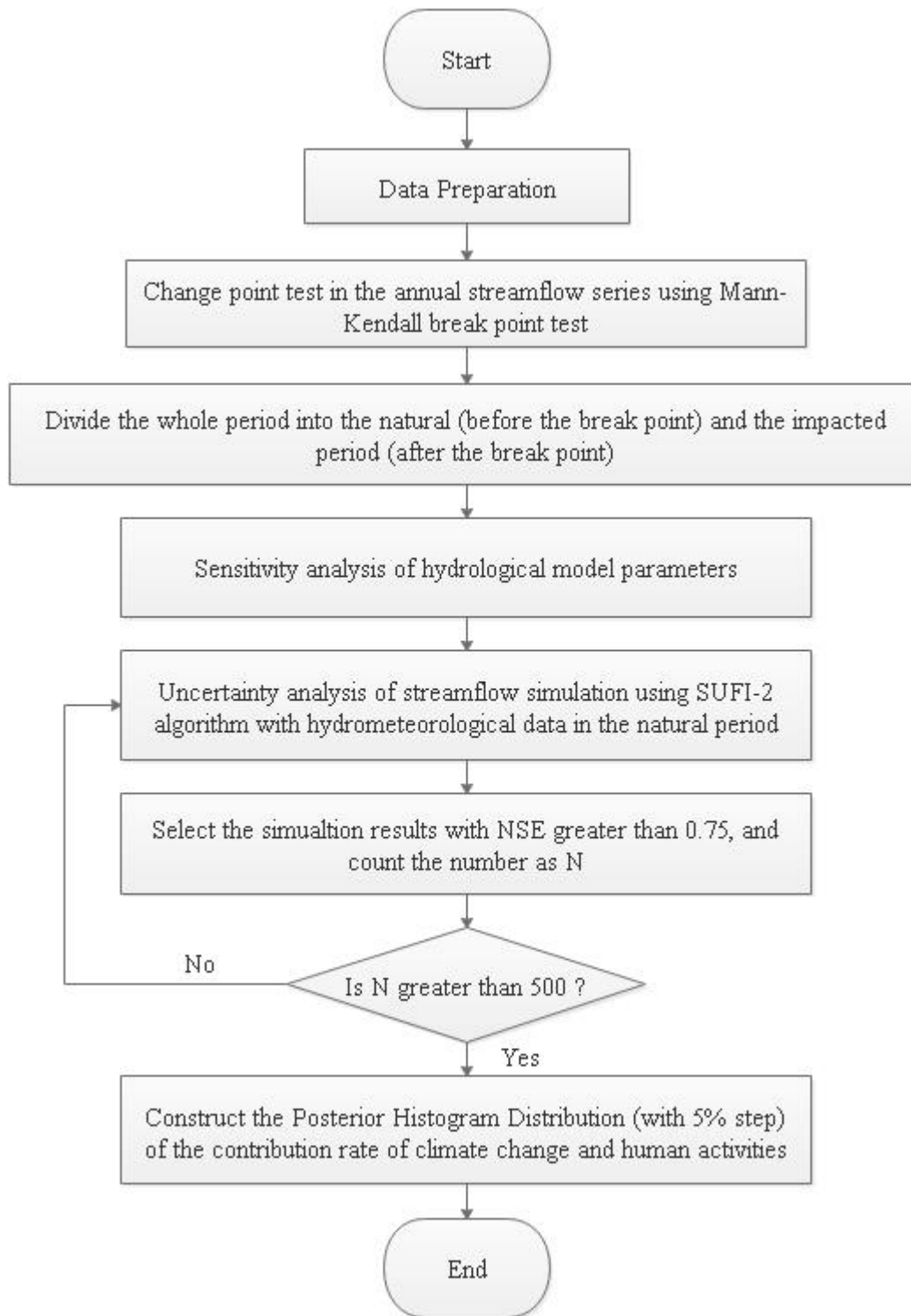
Fig. 2. Flowchart of the newly proposed quantitative framework.

3.2 Mann-Kendall test

In this step, the trends and break points of the hydrometeorological data are detected using the nonparametric Mann-Kendall
200 monotonic trend test (Gilbert, 1987; Kendall, 1975; Mann, 1945) and the Mann-Kendall break point test (Sneyers, 1991),

respectively. The main consideration of using the Mann-Kendall test is that this method assumes no particular distribution for the tested time series (Song et al., 2019; Xu et al., 2018). Significance levels of α = 0.01 and 0.05 is used in this study.

3.2.1 Mann-Kendall monotonic trend test

The Mann-Kendall (MK) monotonic trend test was developed by Mann (1945), Kendall (1975) and Gilbert (1987), which has been widely used to detect the presence of an upward or downward trend of the hydrometeorological time series, and the advantage of this test is that the time series does not need to follow a certain distribution (Hamed and Ramachandra Rao, 1998). This method first tests whether to reject the null hypothesis (H_0: no monotonic trend) and accept the alternative hypothesis (H_a: with monotonic trend) for a significance level of α. The defined statistic S can be calculated by the following equation:

$$S = \sum_{k=1}^{n-1} \sum_{j=k+1}^{n} sign(x_j - x_k) \tag{1}$$

where x_k is the data in the order over time, x_1, x_2, …, x_{n-1}, which means the time series obtained at times 1, 2, …, n-1, respectively; x_j is another time series over time x_{k+1}, x_{k+2}, …, x_n; n is the length of the data set record; and $sign(x_j - x_k)$ is a sign function that takes on the values of 1, 0, or -1 based on the sign of $x_j - x_k$, and its values can be calculated by the following equation:

$$sign(x_j - x_k) = \begin{cases} -1, & x_j - x_k < 0 \\ 0, & x_j - x_k = 0 \\ 1, & x_j - x_k > 0 \end{cases} \tag{2}$$

After calculating the S sequence, the variance of S can be computed as follows:

$$VAR(S) = \frac{1}{18} \left[n(n-1)(2n+5) - \sum_{p-1}^{g} t_p(t_p - 1)(2t_p + 5) \right] \tag{3}$$

where n is the length of the time series; g is the length of any given tied group and t_p is the length of the data set series in the p_{th} group. Then, the defined test statistic Z_{MK} can be transformed from the statistical value S, and the equation is as follows:

$$Z_{MK} = \begin{cases} = \dfrac{S-1}{\sqrt{VAR(S)}} & if\ S > 0 \\ = \quad 0 & if\ S = 0 \\ = \dfrac{S+1}{\sqrt{VAR(S)}} & if\ S < 0 \end{cases} \tag{4}$$

At the given significance level α, if $-Z_{\alpha/2} \leq Z_{MK} \leq Z_{\alpha/2}$, then the H_0 (null hypothesis) is accepted, which means that there is no significant trend in the time series. By contrast, a positive Z_{MK} indicates that the tested time series has an upward trend, while a negative value indicates a downward trend.

3.2.2 Mann-Kendall break point test

The break point of the hydrometeorological time series denotes a change from one stable state to another stable state (Xu et al., 2018). It occurs when the climate system breaks through a certain threshold. The Mann-Kendall break point test has been widely used to test break points for hydrometeorological time series, signaling when abrupt changes start (Sneyers, 1991). This test method is used to determine the break point of the observed annual streamflow in this study. The defined statistic UF_k is obtained by the following formulas:

$$UF_k = \frac{S_k - E(S_k)}{\sqrt{Var(S_k)}} \qquad k = 1, 2, ..., n \tag{5}$$

$$S_k = \sum_{i=1}^{k} r_i \qquad r_i = \begin{cases} 1 & x_i > x_j \\ 0 & else \end{cases} \qquad j = 1, 2, ..., i \tag{6}$$

where x_i is the variable to be tested and n is the total number of data points. The expectation $E(S_k)$ and variance $Var(S_k)$ of the data series can be calculated as follows:

$$E(S_k) = \frac{n(n-1)}{4} \tag{7}$$

$$Var(S_k) = \frac{n(n-1)(2n+5)}{72} \tag{8}$$

UF_k is a sequence of statistics calculated by arranging x_1, x_2, ..., x_n in the order of time series x that obeys the standard normal distribution. Then, treating the time series x in reverse order x_n, x_{n-1}, ..., x_1, the above process is repeated, but by using a reversed definition of $UB_k = -UF_k, k = n, n-1, ..., 1$. Given the significance level α (0.01 in this study), if $UB_k = -UF_k, k = 1, 2, ..., n$, no significant trend is detected, where $U_{\alpha/2}$ is the standard normal deviation. In contrast, this means that the tested sequence has a significant upward or downward trend when $|UF_k| > U_{\alpha/2}$. Then, the curves of UF_k and UB_k are plotted. If there is an intersection of the two curves and the trend of the data series is statistically significant, then this intersection is regarded as the break point of the data series.

After identification of the break points in the annual streamflow series, the study period is divided into a "natural period" (before the break point) and an "impacted period" (after the break point) (Wang et al., 2015; Bao et al., 2012). The "natural period" means that there is no significant increase or decrease in streamflow during this period, and it also means that relatively slow CC is the dominant factor, and that the impact of HAs is very small during this period. Consequently, the impacted period indicates to a significant change in streamflow during this period, mostly due to factors such as the construction of water conservancy engineering facilities, increased water consumption for irrigation, changes in land use and increased water consumption in cities and towns.

3.3 SWAT model

The Soil & Water Assessment Tool (SWAT) model is a semi-distributed, physical process-based hydrological model developed by the Agricultural Research Service of the United States Department of Agriculture (USDA-ARS) (Arnold et al., 1998). The SWAT model first divides the study area into several subbasins based on DEM data, and then each subbasin is further divided into several HRUs (Hydrologic Response Units) based on land use and soil data sets. Then, streamflow generation at the subbasin scale is calculated following the principles of water balance and energy balance after inputting the meteorological data sets. Finally, the total flow of river basin exports is calculated according to the Muskingum method (Tang et al., 2019; Arnold et al., 2012b). We chose to use the SWAT model in this study because numerous published studies have proven that this model has excellent performance in hydrological simulations across the world (Tang et al., 2019; Zhao et al., 2018a; Zhao et al., 2018b; Lee et al., 2018).

The calibration of model parameters is executed using the independent software SWAT-CUP, which was developed by Abbaspour et al. (2007). This software is freely available and provides five parameter calibration and uncertainty analysis methods. In this study, the sequential uncertainty domain parameter fitting version 2 (SUFI-2) algorithm (Abbaspour et al., 1997; Abbaspour et al., 2004) was used to perform parameter calibration and uncertainty analysis, because this method has proven to have the advantages of shorter calculation time, ease of implementation and ability to set arbitrary objective functions (Zhao et al., 2018a; Tuo et al., 2016; Wu and Chen, 2015). The performance of the SWAT model was evaluated by the Nash-Sutcliffe efficiency coefficient (NSE) (Nash and Sutcliffe, 1970) and relative error (RE):

$$\text{NSE} = 1 - \frac{\sum_{i=1}^{N}\left(Q_{obs,i} - Q_{sim,i}\right)^2}{\sum_{i=1}^{N}\left(Q_{obs,i} - \overline{Q_{obs}}\right)^2} \tag{9}$$

$$\text{RE} = \frac{R_{sim} - R_{obs}}{R_{obs}} \times 100\% \tag{10}$$

where $Q_{obs,i}$ and $Q_{sim,i}$ are the observed and simulated streamflow, respectively; $\overline{Q_{obs}}$ is the mean value of the observed streamflow; N is the total number of days or months in the calibration period; and R_{sim} and R_{obs} are the mean annual simulated and observed streamflow, respectively.

3.4 Construction of the Posterior Histogram Distribution of contribution rate

In this section, we introduce how to calculate the CR of climate change (CC) and human activities (HAs) to streamflow variations and how to construct the posterior histogram distribution (PHD) of the CR to consider the uncertainty of hydrological simulations.

3.4.1 CR of CC and HAs

A schematic diagram of the attribution evaluation of streamflow changes is shown in Fig, 3. ΔQ in the figure represents the amount of change in the observed streamflow during the impacted period based on the natural period, while ΔQ_{cc} and ΔQ_{ha} represent the amount of streamflow change caused by CC and HAs, respectively. The total change in the annual streamflow can be calculated using the following formula:

$$\Delta Q = \Delta Q_{cc} + \Delta Q_{ha} = \overline{Q_{oi}} - \overline{Q_{on}} \tag{11}$$

where $\overline{Q_{oi}}$ and $\overline{Q_{on}}$ are the mean annual observed streamflow (m³/s) in the impacted period and natural period, respectively.
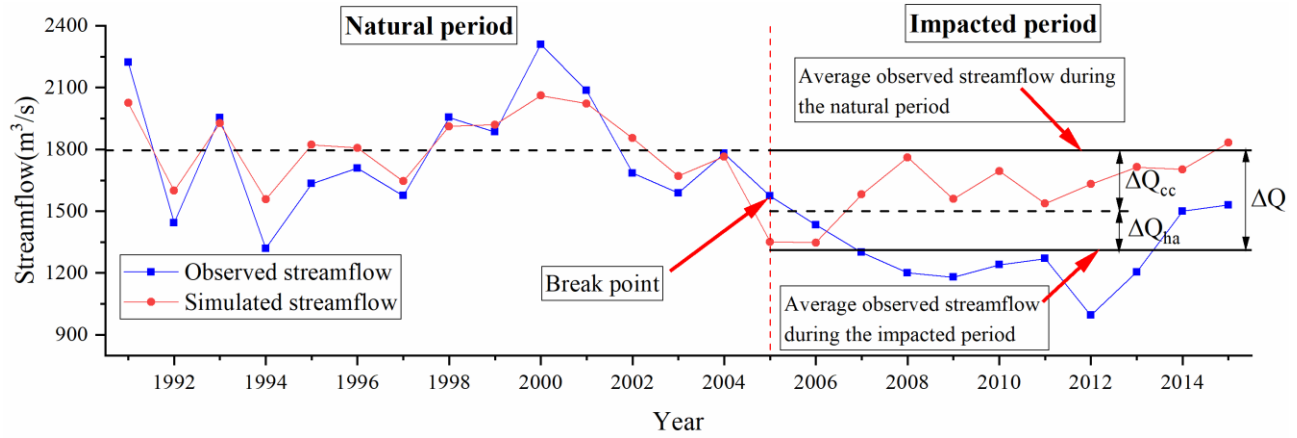
Fig. 3. Schematic diagram of the contribution rate (CR) of climate change (CC) and human activities (HAs) to streamflow change using SWAT modelling. (Notation: ΔQ, ΔQ_{cc} and ΔQ_{ha} respectively represent the amount of streamflow change in the impacted period, the amount of streamflow change caused by CC, and the amount of streamflow change caused by human activities.)

The hydrological and meteorological data in the natural period are input into the SWAT model, and using the SUFI-2 method to calibrate the model, a set of parameters represents the characteristics of catchment under natural conditions with less impact from HAs. Then, this set of parameters is brought back into the SWAT model using the meteorological data of the impacted period. Based on the above simulation results, the CC induced in streamflow can be calculated as follows:

$$\Delta Q_{cc} = \overline{Q_{si}} - \overline{Q_{sn}} \tag{12}$$

where $\overline{Q_{si}}$ and $\overline{Q_{sn}}$ represent the mean simulated annual streamflow (m³/s) for the impacted period and natural period, respectively. Thus, the streamflow change induced by HAs can be calculated by the following equation:

$$\Delta Q_{ha} = \Delta Q - \Delta Q_{cc} \tag{13}$$

After the calculation of ΔQ_{cc} and ΔQ_{ha}, the CR of CC and HAs to streamflow changes, which are defined as CR_{cc} and CR_{ha}, respectively, can be estimated as:

$$CR_{cc} = \frac{|\Delta Q_{cc}|}{|\Delta Q|} \times 100\% \tag{14}$$

$$CR_{ha} = \frac{|\Delta Q_{ha}|}{|\Delta Q|} \times 100\% \tag{15}$$

Equations 12 to 15 are also applicable to quantify the CR of CC and HAs to streamflow changes on a monthly scale.

3.4.2 Construction of the PHD of the CR of CC and HAs

Before the construction of the PHD of the CR of CC and HAs, the sensitivity of the parameters of the SWAT model is first conducted. Based on the related published literature (Zhao et al., 2018a; Yang et al., 2008; Malagò et al., 2015) and the authors' experience, the Latin-Hypercube and global sensitivity methods were used to perform the uncertainty analysis (Abbaspour et al., 2007). The global sensitivity analysis method is the estimation of the average change in the objective function caused by the change in each parameter, and all parameters change during the whole process. A t-test was used to identify the relative sensitivity of each parameter. Considering the influence of the snowmelt streamflow process upstream of the LR Basin on the hydrological

simulation, 22 parameters were selected and the details of these selected parameters are shown in Table 2. According to the suggestion of Abbaspour et al. (2004), 500 simulations were set up to implement the sensitivity analysis. The t-stat and P-values were used to measure which parameters were more sensitive, where a larger absolute t-stat value and a smaller absolute P-value represent a higher sensitivity of a given parameter.

310   **Table 2** Twenty-two selected SWAT model parameters in the sensitivity analysis at Yunjinghong station

Parameter	Description	Parameter Range
R_CN2	SCS runoff curve number for soil condition II	−0.2 – 0.2
R_SOL_AWC	Available water capacity of each soil layer	−0.2 – 0.1
A_GWQMN	Threshold depth of water in the shallow aquifer required for return flow to occur	0 – 25
V_SNOCOVMX	Minimum snow water content that corresponds to 100% snow cover	0 – 500
V_SMFMN	Minimum melt rate for snow during the year (occurs on the winter solstice)	0 – 20
V_CH_K2	Effective hydraulic conductivity in the main channel alluvium	0 – 500
V_GW_REVAP	Groundwater "revap" coefficient	0.02 – 0.2
V_REVAPMN	Threshold depth of water in the shallow aquifer for "revap" to occur	0 – 500
V_GW_DELAY	Groundwater delay (days)	0 – 500
V_ALPHA_BF	Baseflow alpha factor (days)	0 – 1
V_SOL_BD	Moist bulk density	0.9 – 2.5
A_ESCO	Soil evaporation compensation factor	0 – 0.2
V_OV_N	Manning's "n" value for overland flow	−0.01 – 0.6
R_RCHRG_DP	Deep aquifer percolation fraction	0 – 1
V_CH_N2	Manning's "n" value for the main channel	0.018 – 0.15
R_SLSUBBSN	Average slope length	0 – 0.2
V_SMTMP	Snowmelt base temperature	−5 – 5
V_TLAPS	Temperature lapse rate	−10 – 10
V_SMFMX	Maximum melt rate for snow during year	0 – 20
R_SOL_K	Saturated hydraulic conductivity	−0.8 – 0.8
V_SFTMP	Snowfall temperature	−5 – 5
V_ALPHA_BNK	Baseflow alpha factor for bank storage	0 – 1

(Notation: R_, V_, and A_ represent multiplying, replacing, and adding the corresponding parameter values, respectively, in the process of calibrating the parameters.)

Based on the sensitivity analysis results, 9 parameters with the highest sensitivity were selected to re-calibrate the model with 1000 simulations. According to the recommendations in Tuo et al. (2016) and Moriasi et al. (2007), the performance of the

315 hydrological simulation can be divided into four grades based on the NSE values: very good performance ($0.75 \leq$ NSE < 1), good performance ($0.65 \leq$ NSE < 0.75), satisfactory performance ($0.5 \leq$ NSE < 0.65) and unsatisfactory performance (NSE < 0.5). According to this evaluation standard, we selected simulation results with NSE greater than 0.75 out of 1000 simulation results to construct the posterior histogram frequency distribution (PHD) of the CR of CC and HAs to streamflow changes using the method introduced in section 3.4.1. Note that to reduce the random error caused by the number of samples, we set the number of

320   simulations with NSEs ≥ 0.75 to be more than 500; that is, we needed to repeatedly use Latin hypercube sampling and the SUFI-2 algorithm until the number of simulation results that met the conditions was more than 500. Then, the CR of more than 500 groups of CC and HAs to streamflow change was calculated. Finally, the posterior histogram distribution (PHD) of the CR of CC and HAs was constructed in 5% steps. At this stage, the histogram column with the highest frequency in the PHD was selected as the result of quantitative analysis, which considered the uncertainty, and the arithmetic average of all results in the column was

325   used as the actual value of the CR of CC and HAs.

3.5 Comparison of the newly developed quantification method with other two methods

    In order to evaluate the calculation accuracy of the novel framework proposed in this study to quantify the CR of CC and HAs to streamflow changes, the Budyko framework was used first. This framework was developed by Budyko (1961) and links climate variability to streamflow (Q) and actual evapotranspiration (AE) through the assumption that the long-term average annual

330   catchment AE is determined by the catchment average precipitation (P) and the catchment potential evapotranspiration (PET) (Liu and Liang, 2015). Over the past few decades, the Budyko framework and its variants have been widely used to conduct CC and HA attribution analyses of streamflow changes (Liu et al., 2017; Han et al., 2019; Xin et al., 2019). According to its theoretical assumptions, the multiyear average water balance within the catchment can be expressed as follows:

$$\Delta S = P - AE - Q \tag{16}$$

335   where P, Q, and AE represent the multiyear average precipitation (mm), streamflow (mm) and actual evapotranspiration (mm), respectively; ΔS (mm) is the change in the amount of water storage at the watershed scale, and it is reasonable to assume that it is equal to 0 on the multiyear average scale. According to Zhang et al. (2001), the AE can be calculated by the following formula:

$$\frac{AE}{P} = \frac{1 + \omega\left(PET/_P\right)}{1 + \omega\left(PET/_P\right) + \left(PET/_P\right)^{-1}} \tag{17}$$

where ω is the plant-available water coefficient which is related to the vegetation type of the catchment. According to the method

340   for selecting the value of ω provided in Zhang's research (Zhang et al., 2001), and based on the multi-year average AE/P (0.55) and PET/P (0.96) values in the LR Basin, this study set the value of ω to 0.5.

    The changes in the catchment streamflow due to CC, which are mainly characterized by precipitation (P) and actual evapotranspiration (AE), can be expressed as follows:

$$\Delta Q_{cc} = \alpha\Delta P + \beta\Delta AE \tag{18}$$

345   where ΔQ_{cc} (mm) represents the streamflow changes induced by CC; α and β represent the sensitivity of streamflow to precipitation and actual evapotranspiration, respectively; and ΔP and ΔAE are the changes in precipitation and actual evapotranspiration in the impacted period compared to the natural period, respectively. The sensitivity coefficients α and β are defined as follows:

$$\alpha = \frac{1 + 2DI + 3\omega DI}{(1 + DI + \omega(DI)^2)^2} \tag{19}$$

350

$$\beta = -\frac{1 + 2\omega DI}{(1 + DI + \omega(DI)^2)^2} \tag{20}$$

where DI is the dryness index which is equal to PET/P.

    Through the above formulas, we can separate the CR of CC to streamflow variations, and further compare it with the calculation results of the new method proposed in this paper.

In addition to the Budyko framework, we also used the GMSWU data introduced in Section 2.2 and the reservoir dead storage capacity data to roughly separate the CR of HAs from the streamflow changes in the LR Basin. The GMSWU data set provides five types of water withdrawals (i.e., irrigation, livestock, domestic use, mining, and manufacturing) within the period of 1970 to 2010 in the LR Basin, and it was generated by downscaling country-scale estimates of different sectoral water withdrawals from the Food and Agriculture Organization (FAO) of the United Nations AQUASTAT, which ensured its good accuracy (Huang et al., 2018). Here, AQUASTAT refers to FAO's Global Information System on Water and Agriculture (http://www.fao.org/aquastat/en/). Catchment-scale annual water use data were calculated by spatially averaging all grids within the LR Basin, and then streamflow changes caused by each type of water use were obtained using the average annual water use value during the impacted period minus that during the natural period. As shown by Han et al. (2019) and Zhao et al. (2012), during the past two decades, dam construction has been the most significant HA affecting the streamflow changes in the LR Basin. Therefore, in this study, we converted the dead storage capacity of 6 large reservoirs (Table 1) into units of millimeters according to their watershed control area because the impact of the reservoir on the outlet flow of the watershed can be used as its minimum impact value on the multiyear average scale. It should be pointed out that here we use two seemingly simpler methods to verify the computational results of the new framework proposed in this study. However, this does not reduce the innovation of this study, as the new framework has the following significant advantages over the other two methods: 1) The new framework can perform quantitative calculations on the annual and monthly scales; 2) It has relatively less data requirements; 3) It has a more explicit physical meaning.

4. Results

4.1 Hydrological and Meteorological trends in the LR Basin

4.1.1 Trends and break points of the streamflow

The results of the Mann-Kendall break point test for the annual streamflow at Yunjinghong station within the period from 1961 to 2015 are shown in Fig. 4. Since the intersection of the UF and UB curves in Fig. 4 is within the confidence intervals (of 0.05 and 0.01), the break point of the annual streamflow in the LR Basin occurred in 2005. Combined with the construction of reservoirs in the LR Basin, the construction of the Xiaowan hydropower station started in October 2004 (with total storage capacity = 15.3 km³). Therefore, according to the principle of time division introduced in Section 3.1, the study period can be divided into the natural period (from 1961 to 2004) and the impacted period (from 2005 to 2015). UF curves of the MK break point test represent the trend of the time series. As shown in Fig. 4, the observed annual streamflow at Yunjinghong station had an increasing trend before 1967, after which the annual streamflow experienced a significant decreasing trend until 2015.
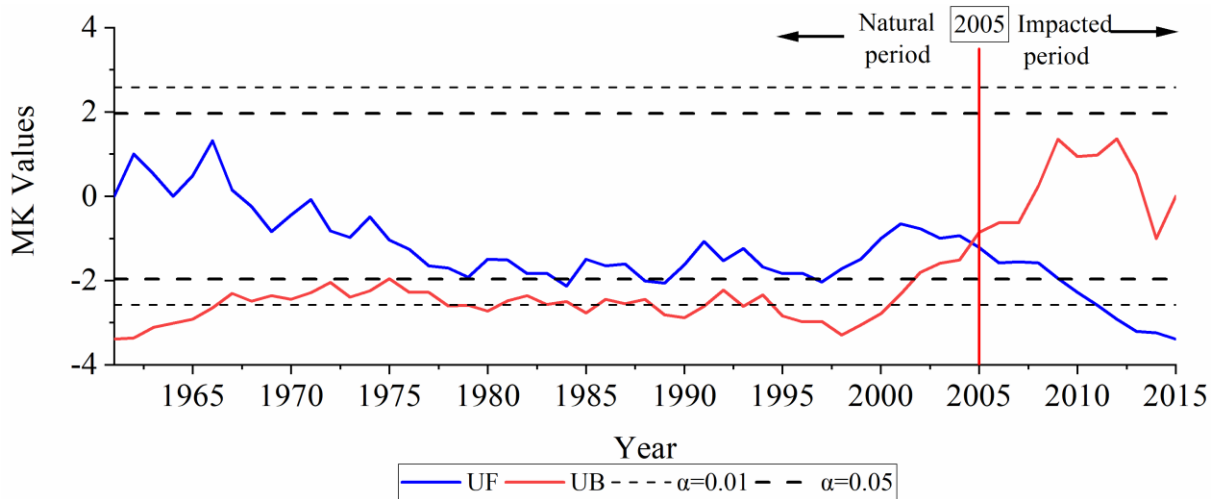
Fig. 4. The Mann-Kendall break point testing statistics of the annual streamflow for the LR Basin from 1961 to 2015.

Fig. 5 shows the MK monotonic trend testing statistics of the annual and monthly streamflow for the LR Basin from 1961 to
385   2015. A positive Z statistic represents an upward trend in the time series, and vice versa. The annual average streamflow in the LR Basin showed a significant decreasing trend, and passed the 0.01 significance level. This decreasing trend of the annual streamflow in the LR Basin is consistent with the conclusions of Han et al. (2019). For the monthly streamflow, the streamflow from February to May showed an increasing trend, among which March and May passed the significance level of 0.05 (with the Z statistic greater than 1.96). The streamflow in the remaining months showed a decreasing trend. Except for June, the decreases
390   in the other months all passed the 0.05 significance level. The decrease in the streamflow from August to October even passed the 0.01 significance test. Among them, the largest decrease was in August (Z statistic = -4.23). This trend of changes in streamflow during the year was mainly caused by the operation of reservoirs within the basin, because reservoirs often release flows during dry periods (from January to May) to alleviate possible droughts in the downstream areas, and they store water during wet periods (from June to October) to reduce the flood control pressure in the downstream area below the reservoir.

395
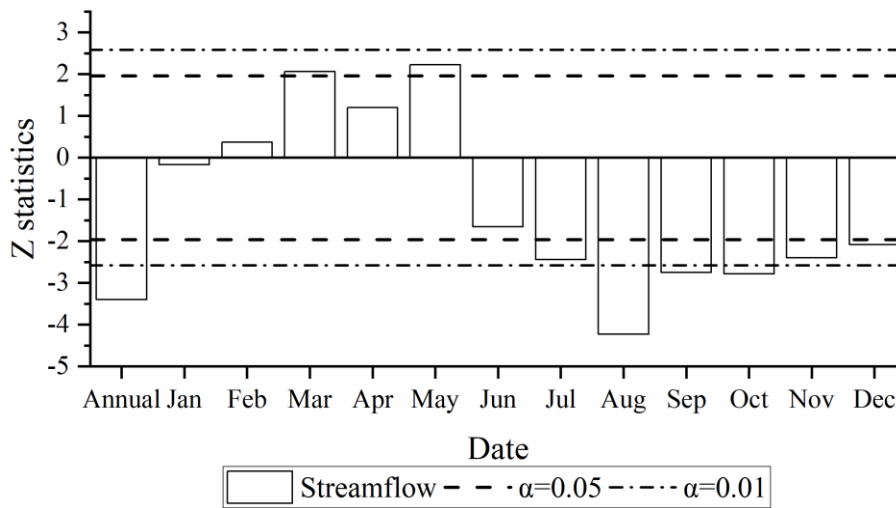
Fig. 5. The Mann-Kendall monotonic trend test statistics of the annual and monthly streamflow for the LR Basin from 1961 to 2015.

4.1.2 Trends and break points of the mean areal precipitation and temperature

The time series and MK break point test results of the annual areal precipitation and mean temperature for the LR Basin from 1961 to 2015 are presented in Fig. 6. In general, changes in the annual precipitation were more complicated than changes in the mean temperature in the LR Basin. The precipitation showed a fluctuating trend, while the mean temperature almost showed a continuous rising trend throughout the study period.

As shown by the time series of the annual precipitation in the LR Basin in Fig. 6 (a), there was a slightly decreasing trend in the LRB during the last 55 years, especially in the past 10 years, but this trend was not significant according to the result of the MK test at the α = 0.05 significance level. The areal annual precipitation in 1985 reached 971 mm, which was the highest in the last 55 years. In 2009, it was 769 mm, which was the lowest value from 1961 to 2015. The MK break point test results showed that there were 11 break points in the annual precipitation time series. Regarding the positive and negative changes in the UF value, the annual precipitation showed a fluctuating trend from 1961 to 1966; then until 1998, the annual precipitation showed a small decreasing trend (except in 1991); from 1999 to 2006, the annual precipitation experienced a small increase; and in the last 9 years (2007-2015), the annual precipitation in the study area showed a decreasing trend.
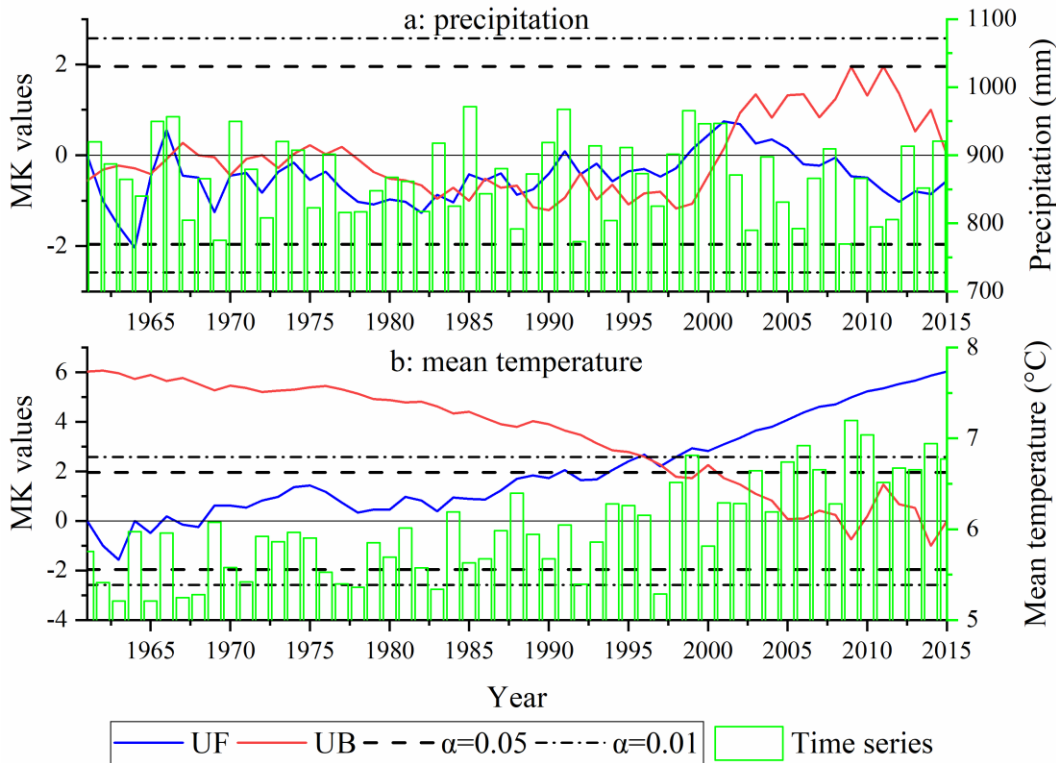
Fig. 6. Time series and the Mann-Kendall break point test statistics of the annual precipitation (a) and mean temperature (b) in the LR Basin from 1961 to 2015.

The time series of the annual mean temperature in the LR Basin presented in Fig. 6 (b) shows that the annual mean temperature in the study area changed relatively smoothly before 1998. After 1998, the temperature began to rise significantly and exceeded the significance level of 0.01. The annual mean temperature in 1963 reached 5.2 ℃, the coldest temperature in the study period. The hottest year was 2009, during which the mean temperature was 7.2 ℃. In terms of changes in the UF value, the mean temperature showed a fluctuating trend from 1961 to 1968, and then continued to rise until it exceeded the significance level

of 0.05 in 1991 and exceeded the significance level of 0.01 in 1998. The break point of the annual mean temperature was detected in 1997.

The MK monotonic trend test statistics of the annual and monthly precipitation and mean temperature for the LR Basin from 1961 to 2015 are presented in Fig. 7. The annual precipitation in the study area showed an insignificant decreasing trend (Z statistic = -0.55), while the annual average temperature showed a significant increasing trend (Z statistic = 6.02) and exceeded the significance level of 0.01. The monthly change in precipitation also showed a fluctuating trend. The increasing trend of precipitation in April and the decreasing trend of precipitation in June exceeded the significance level of 0.05, while the trends of precipitation in other months were not significant (|z statistic| < 1.96). The trend of the monthly mean temperature was relatively simple. Except for the increase in the mean temperature in November, which passed the significance level of 0.05, the increasing trend of the mean temperature in all other months passed the significance level test of 0.01. This also means that the climate in the study area has been gradually warming and drying during the past 55 years.
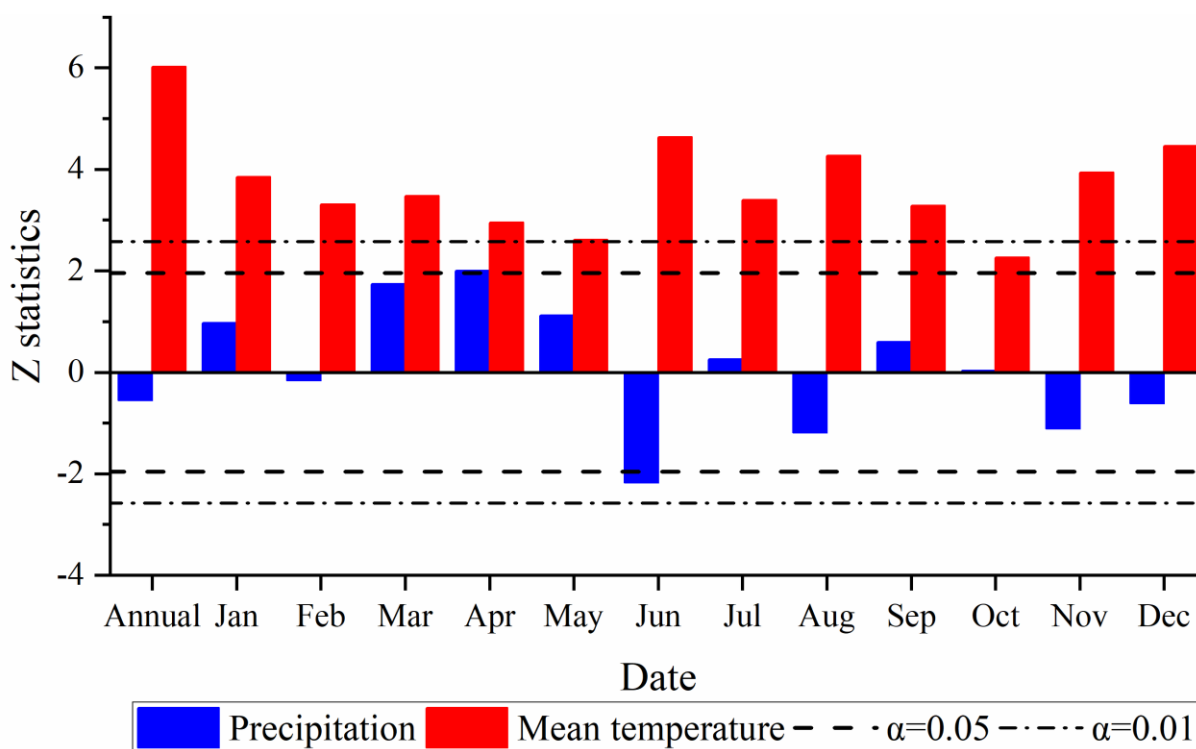
Fig. 7. The Mann-Kendall monotonic trend test statistics of the annual and monthly precipitation and mean temperature for the LR Basin from 1961 to 2015.

4.2 Results of the SWAT simulations

4.2.1 Sensitivity analysis of the SWAT model parameters

As described in Section 3.4.2, the sensitivity of 22 selected parameters was evaluated using the SWAT-CUP software (Abbaspour et al., 2007; Abbaspour et al., 1997), and this software integrates the global sensitivity analysis method and the parameter optimization methods (such as SUFI-2). The SWAT-CUP can perform a combined optimization and uncertainty analysis using a global search procedure and deal with a large number of parameters through Latin hypercube sampling. The

sensitivity evaluation indexes, the t-Stat and P-value, of 22 parameters are shown in Table 3. Obviously, the sensitivity ranks of
the parameters calculated based on SUFI-2 showed that ALPHA_BNK has the highest sensitivity, followed by CH_K2, SOL_BD, GW_REVAP, SFTMP, CN2, SOL_K, SMTMP and ALPHA_BF, whereas the other 14 parameters have less sensitivity for the streamflow simulation. ALPHA_BNK mainly controls the baseflow process within the watershed, and this parameter has also proven to have high sensitivity in other relevant studies (Wu and Chen, 2015), especially in mountainous areas. CH_K2 and ALPHA_BF are mainly related to groundwater runoff, CN2 is the SCS runoff curve number, and these parameters all have higher sensitivity in many published articles on the SWAT model parameter sensitivity (Zhao et al., 2018a; Wu and Chen, 2015). Other parameters with high sensitivity, such as SFTMP and SMTMP, which mainly control the snowmelt process in the basin, also indicate that snowmelt runoff plays an important role in the recharge of the LR Basin (Gao et al., 2019). Based on the above sensitivity analysis results, the top 9 parameters of the sensitivity ranking were selected for further research.

Table 3 Basin wide sensitivity ranking calculated from 22 selected parameters using SUFI-2

Parameter	t-Stat	P-Value	Parameter	t-Stat	P-Value
V_ALPHA_BNK	38.1	0	V_CH_N2	1.25	0.21
V_CH_K2	-10.5	0	V_TLAPS	1.19	0.23
V_SOL_BD	6.81	0	A_ESCO	1.12	0.24
V_GW_REVAP	-5.0	0	V_SNOCOVMX	-1.01	0.31
V_SFTMP	-4.73	0	V_PLAPS	-0.73	0.47
R_CN2	4.60	0	V_GW_DELAY	-0.68	0.50
R_SOL_K	4.34	0	R_SLSUBBASN	-0.65	0.52
V_SMTMP	3.41	0	V_OV_N	0.44	0.66
V_ALPHA_BF	-2.70	0	V_SMFMX	0.36	0.72
R_SOL_AWC	-2.46	0.01	A_GWQMN	0.15	0.88
R_RCHRG_DP	-1.74	0.08	V_REVAPMN	-0.07	0.94

(Notation: V_ represents replacing the default value with the given value; R_ represents the relative change (%); and A_ represents adding the given value to the original parameter value)

4.2.2 Results of the SWAT simulations

As mentioned above, the 9 parameters with the highest sensitivity rankings that controlled different stages of the basin's streamflow production and flow concentration were selected to re-calibrate the model using the SUFI-2 method, and the number of simulations was set to 2000. To reduce the influence of the initial value of the model parameters on the simulation results, during the model parameter calibration process, 1961 and 1962 were set as the warming-up period. Table 4 shows the evaluation metrics of the simulation using the SWAT model at a monthly scale with the largest NS value. For the calibration period from 1963 to 1990, the NSE and RE were found to be equal to 0.94 and -10.62%, respectively; for the validation period from 1991 to 2004, the model performance was slightly better than that in the calibration period, and the NSE and RE were 0.95 and -8.65%, respectively. For the whole period from 1963 to 2004, the NSE (0.94) and RE (-9.97%) were also satisfactory. According to the requirements of the Information Center of the Ministry of Water Resources, the data provider, this study standardized the observed and simulated runoff curves of the Yunjinghong station. Fig. 8 shows the normalized monthly observed and simulated streamflow at Yunjinghong station from 1963 to 2004 and the histogram of the mean monthly precipitation in the LR Basin. As seen from

Fig. 8 (a) and Fig. 8 (b), the SWAT model can simulate the flow processes very well and almost perfectly match the observed

465   streamflow curve. Note that the simulated streamflow overestimated the floods in individual years (1973, 1985 and 1995 in Fig.8 (b)), which might be caused by the uncertainty of the precipitation product (Han et al., 2019). In summary, the SWAT model can better simulate the streamflow process at Yunjinghong station on a monthly scale; therefore, this model is considered suitable for the next part of the research.

Table 4 Evaluation metrics, Nash-Suttcliffe Efficiency and Relative Error of the SWAT model on a monthly scale

Period	NSE	RE (%)
Calibration (1963-1990)	0.94	-10.62
Validation (1991-2004)	0.95	-8.65
Overall (1963-2004)	0.94	-9.97

470
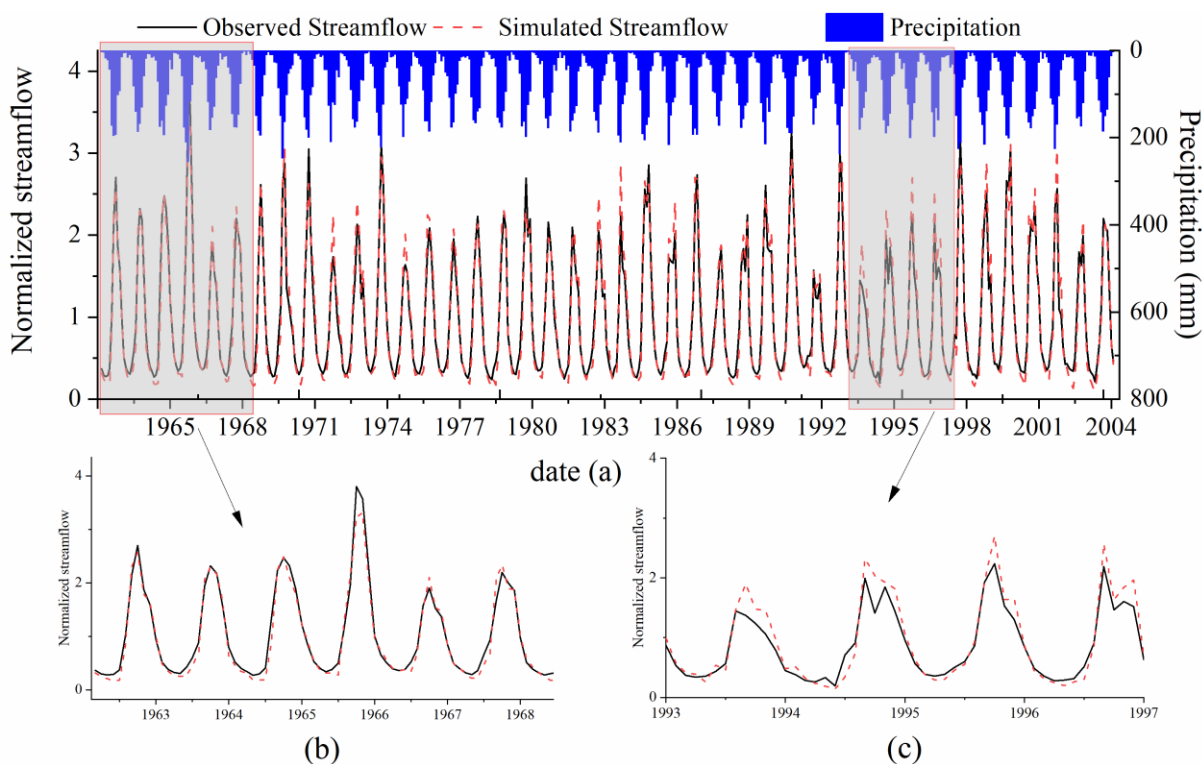
Fig. 8. Normalized monthly observed and simulated streamflow at Yunjinghong station for the calibration (from 1963 to 1990) and validation (from 1991 to 2004) periods. The blue histogram shows the monthly precipitation in the LR Basin. The normalized streamflow was calculated from the observed and simulated streamflow divided by their average values.

475   According to the method described in Section 3.4.2, simulations with NSEs greater than 0.75 among the 1000 simulations were selected. Fig. 9 shows the number of simulations with $0.75 \leq NSE < 0.8$, $0.8 \leq NSE < 0.85$, $0.85 \leq NSE < 0.9$ and $0.9 \leq NSE < 0.95$ during the calibration period (1963 - 1990), the validation period (1991 - 2004) and the whole period (1963 - 2004) on a monthly scale. In summary, there were 575 simulations with NSEs greater than 0.75 out of 1000 simulation results during the calibration period, the validation period, and the whole period. Clearly, the NSEs of most simulation results were between 0.75

480   and 0.9, with 533, 537 and 533 simulations in the calibration period, the validation period, and the whole period, respectively, and

only a few simulation results had NSEs greater than 0.9. In the different periods, the model performed well in the validation period compared with that in the calibration period, which indicated that the model has good predictive ability in the LR Basin.
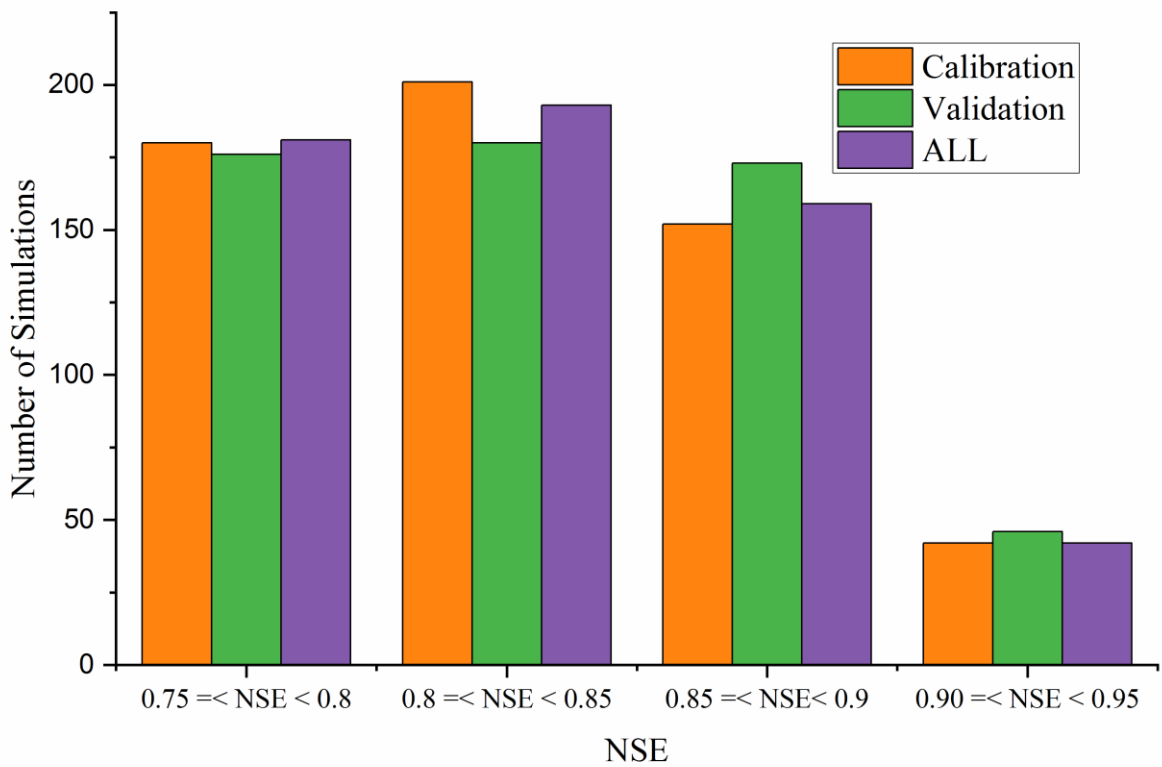
Fig. 9. Number of simulations with NSEs greater than 0.75 during the calibration (1963 - 1990), validation (1991 - 2004), and whole periods (1963 - 2004).

4.3 Quantification of CC and HAs for streamflow change considering the uncertainties

4.3.1 Quantification of the impacts considering the uncertainties at the annual scale

The 575 simulations with NSEs greater than 0.75 were selected to construct the posterior histogram frequency distribution (PHD) of the CR of CC and HAs to streamflow changes in the LR Basin. Fig. 10 shows the number of simulations of the CC CR in 5% intervals and their corresponding NS box plots. In total, 167 out of 575 simulations calculated that the CR of CC in the LR Basin to runoff reduction was 40% - 45%, and the average NSE was 0.84. Then, 131 and 92 of the simulation results had calculated climate CRs of 35 - 40% and 45 - 50%, respectively. The CR of CC in other intervals had relatively few simulations. The NSE value of the CR between 70-75% was the largest (NSE = 0.86), but it had only 1 simulation. Therefore, when using hydrological simulations to quantify the CR of CC and HAs to the streamflow change of the watershed, not only the merits of the model performance but also the uncertainty of the model simulation should be considered. In general, according to the results calculated by the new quantitative framework proposed in this paper, streamflow changes in the LR Basin duo to CC accounted for 40-45% (with an average CR of 42.6%), and the corresponding HAs accounted for 55-60% (with an average CR of 57.4%).
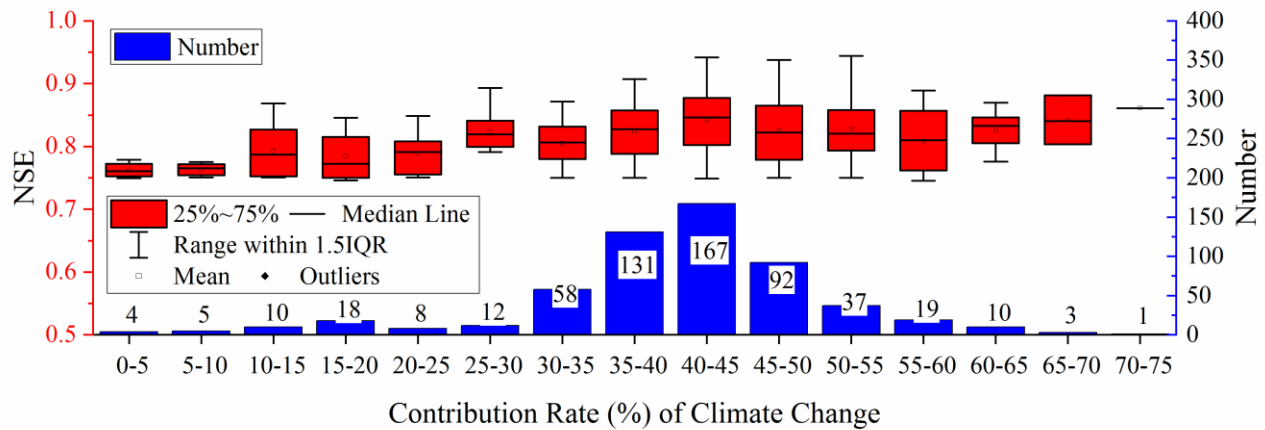
Fig. 10. Histogram of the number of simulations of the CR (with 5% steps) of climate change to streamflow reduction in the LR Basin at the annual scale and corresponding Nash-Sutcliffe Efficiency box plots.

Table 5 shows the average values of the main hydrological and meteorological elements and their changes during the natural period and the impacted period. During the impacted period, compared with the natural period, the multiyear average streamflow decreased by 396 m³/s (86.5 mm), the precipitation decreased by 25 mm; as basin wide temperatures increased, the mean potential evapotranspiration and temperature in the basin increased by 6.4 mm and 0.9°C. In terms of relative changes, the streamflow decreased by 22%, but precipitation and potential evapotranspiration changed by -2.9% and 6.4%, respectively, which may indicate that the streamflow reduction in the LR Basin was mainly caused by HAs.

Table 5 Hydrological and meteorological elements in the natural (1963 - 2004) and impacted periods (2005 - 2015) of the LR Basin and their changes during the two periods

Hydro-meteorological element	Streamflow (m³/s)	Streamflow (mm)	Precipitation (mm)	Potential evapotranspiration (mm)	Temperature (°C)
Natural period	1801.5	398.6	863.8	832.5	5.8
Impacted period	1405.5	312.1	838.8	885.8	6.7
Amount of change	-396	-86.5	-25	53.3	0.9
Relative change (%)	-22.0	-22.0	-2.9	6.4	15.9

4.3.2 Quantification of the impacts considering the uncertainties on a monthly scale

The monthly CR of CC and HAs to the changing streamflow at Yunjinghong station was also analyzed using the new framework proposed in this study, and the results are shown in Fig. 11. In general, only June and November had a large CR of CC, which reached 95 - 99.9% and 70 - 75%, respectively, while the CR of CC in the other 10 months was relatively small. The trends of the streamflow and the precipitation and mean temperature in the study area shown in Fig. 5 and Fig. 7 indicate that the streamflow in June and November showed a decreasing trend (Fig. 5), while the precipitation in June decreased significantly (passing the significance level of 0.05), and the temperature increased significantly (passing the significance level of 0.05) (Fig. 7). This significant decrease in precipitation and the significant increase in temperature were the main reasons for the decrease in

the streamflow in June; that is, the decrease in the streamflow in June was mainly caused by CC. The main factors that led to the decrease in the streamflow in November were also the decrease in precipitation and the significant increase in temperature (Fig. 7). From the results of each month, the CR of CC in March and April was the smallest, reaching 10 - 15%; followed by July (15 - 20%); May, August, and September (20 - 25%); October (25 – 30%); January and February (30 – 35%); and December (45 – 50%).
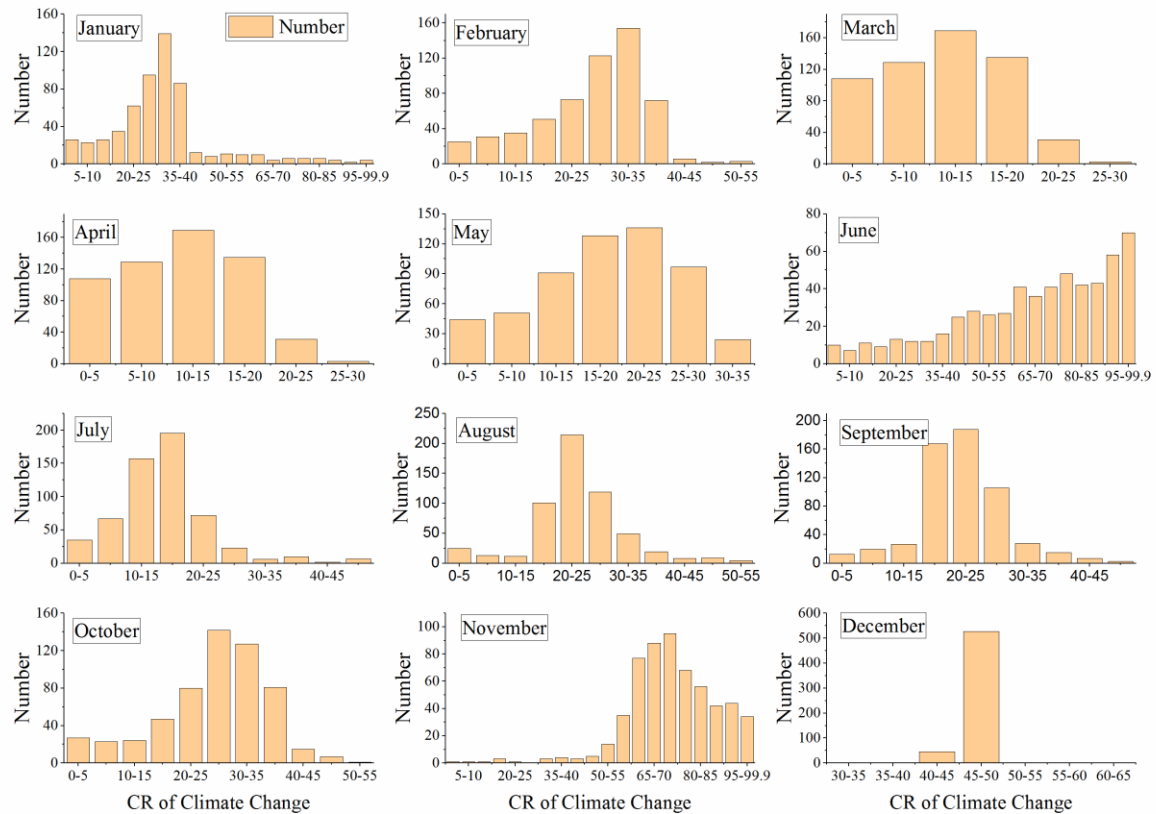
Fig. 11. Histogram of the number of simulations of the contribution rate (CR) (with 5% step) of climate change to streamflow reduction in the LR Basin on a monthly scale.

The mean CR of CC and HAs at the monthly scale, which was calculated by averaging the CRs of all simulation results within the highest frequency, is displayed in Fig. 12 (left panel), and the monthly precipitation, potential evapotranspiration and runoff depth during the natural period and the impacted period are shown in the right panel of Fig. 12. Overall, the monthly CR was consistent with the annual results, and the CR in a total of 10 months was mainly due to HAs that led to a decrease in the streamflow in the LR Basin. It is worth noting that the CR of CC in June reached 96%. The panel in the right of Fig. 12 shows that the precipitation in June during the impacted period was significantly reduced compared with the natural period (with a 20.2 mm decrease). At the same time, the increase in potential evapotranspiration in June was also relatively obvious (with a 9.2 mm increase). Fig. 12 (right panel) clearly shows that the streamflow in the LR Basin during the impacted period was significantly reduced compared with the natural period in June to October, and the precipitation had little change, except in June. Therefore, we can conclude that the main reason for the decrease in the streamflow in the LR Basin was HAs, as shown in the left panel. In

535 this study area, the main cause of the streamflow changes was mainly due to the construction of reservoirs (such as Manwan and Xiaowan), and at the same time, the water storage of these water conservancy facilities during the flood period also provides engineering support for protecting the safety of downstream life and property. Conversely, during the dry season (from January to May), the streamflow in the impacted period showed an increasing trend compared with the natural period, and the increase in runoff during these five months was mainly due to HAs (Fig. 12, left panel), which might have been caused by the release of water

540 from the reservoirs during the dry season. For example, in 2016, due to the influence of El Niño, the countries along the lower Mekong River all suffered severe drought. The Chinese government immediately asked the Jinghong Reservoir to release water urgently, which effectively helped downstream countries mitigate a series of possible effects caused by drought and water shortages (Li et al., 2017b).
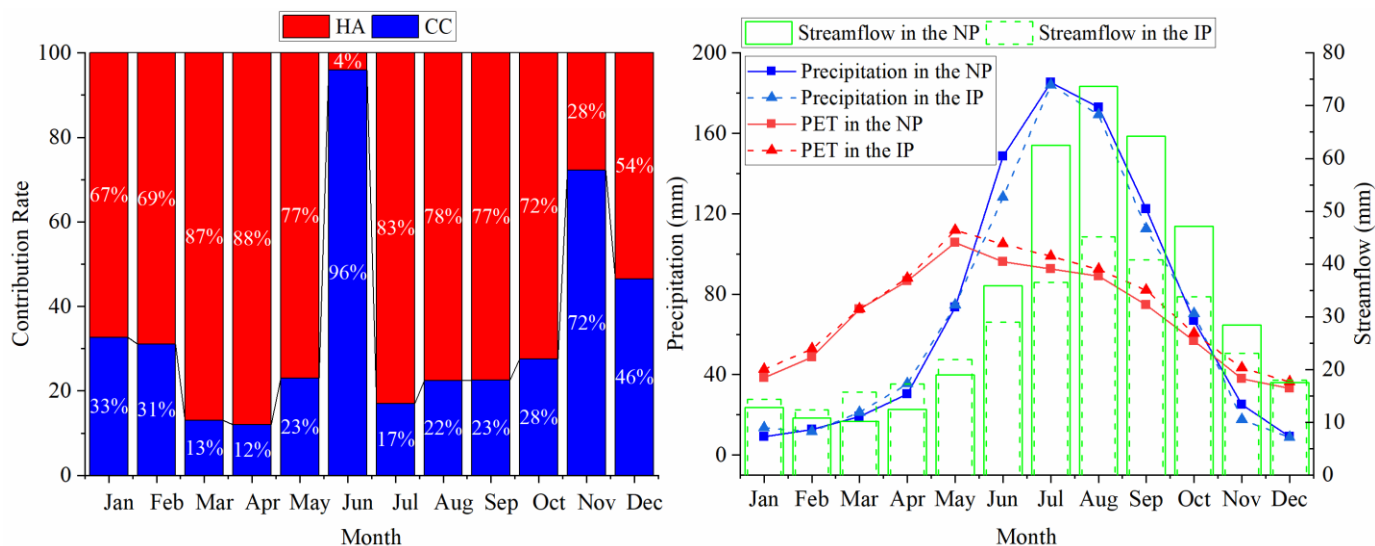
545 **Fig. 12**. CR of CC and human activities to the changing monthly streamflow at Yunjinghong station (left panel), monthly precipitation, potential evapotranspiration and runoff depth during the natural period and the impacted period in the LR Basin (right panel). (Notation: HA = "Human Activities", CC = "Climate Change", PET = "Potential evapotranspiration", NP = Natural Period and IP = Impacted Period)

4.4 Comparison with the other two methods

550 In this sub-section, the new proposed framework that considers the uncertainty of hydrological simulations was compared with the Budyko framework, five sections of water withdrawal data from the LR Basin and the equivalent streamflow depth converted from the dead storage capacity of six large hydropower stations.

 Table 6 shows the CR of CC and HAs to annual streamflow changes at Yunjinghong station, which was calculated from the Budyko framework. The actual evapotranspiration was calculated from the annual precipitation minus the annual streamflow depth. As shown in Table 6, compared with the natural period, the precipitation and streamflow depth in the impacted period

555 showed a decreasing trend.

Table 6 CR of climate change (CC) and human activities (HA) calculated by the Budyko framework

Time period	Precipitation (mm)	Streamflow (mm)	Actual evapotranspiration (mm)	CC (%)	HA (%)

Natural period	863.8	398.6	463.7	37.2	62.8
Impacted period	838.8	312.1	526.6		

The precipitation decreased by 25 mm and the streamflow depth decreased by 86.5 mm. In contrast, the actual evapotranspiration showed an increasing trend, which may be related to the continuous increase in temperature in recent decades.

560 The CR of CC and HAs to streamflow changes accounted for 37.2% and 62.8%, respectively, which was basically consistent with the results calculated by the new framework proposed in this study (the difference was 5.4%).

Fig. 13 shows the annual water withdrawals (i.e., domestic, irrigation, livestock, manufacturing and mining) in the LR Basin during the period from 1970 to 2010 and changes in the installed capacity and dead reservoir storage from 1992 to 2015. In addition to the amount of water use for irrigation, the other four types of water use withdrawals all showed an increasing trend

565 from 1970 to 2010, with domestic water consumption increasing the most (linear slope = 0.043). The comparison between the impacted period and the natural period showed that the other four types of water consumption, except for domestic water use, all had a larger increase in the natural period than during the impacted period. To meet the power generation needs of Southwest China and the flood control and drought resistance requirements of downstream countries, the total dead storage capacity and total installed capacity of the reservoirs from 1992 to 2015 all showed a significant increase, especially after the construction of

570 Nuozhadu hydropower station in 2012, shown in Fig. 1.

According to the method introduced in Section 3.5, the changes in the streamflow caused by HAs in the LR Basin were separated, which mainly included the five sections of water consumption changes and the same amount of water depth as the total dead storage capacity of the reservoir. Fig. 14 shows the CR of the five types of water withdrawals by HAs and the construction of the reservoirs to the streamflow changes in the LR Basin during the impacted period (from 2005 to 2015) compared to the natural period (from 1961 to 2004). Overall, the CR of HAs to streamflow changes was 59.91%, while that of CC was 40.09%. This result was also consistent with the results calculated in Section 4.3.1. Among them, the streamflow depth caused by the construction of the reservoir was reduced by -50.17 mm, which was also the factor that had the greatest impact on streamflow compared with other HAs, and its CR reached 58.0%, while the CR of the other five types of water withdrawal was relatively small. The CRs of domestic, irrigation, livestock, manufacturing, and mining water withdrawals were 1.32%, -0.35%, 0.12%, 0.79% and 0.03%, respectively, a total of 1.91%. In other words, the decrease in the streamflow in the LR Basin was mainly due to the impact of HAs, and most of it was caused by the construction of the reservoirs.
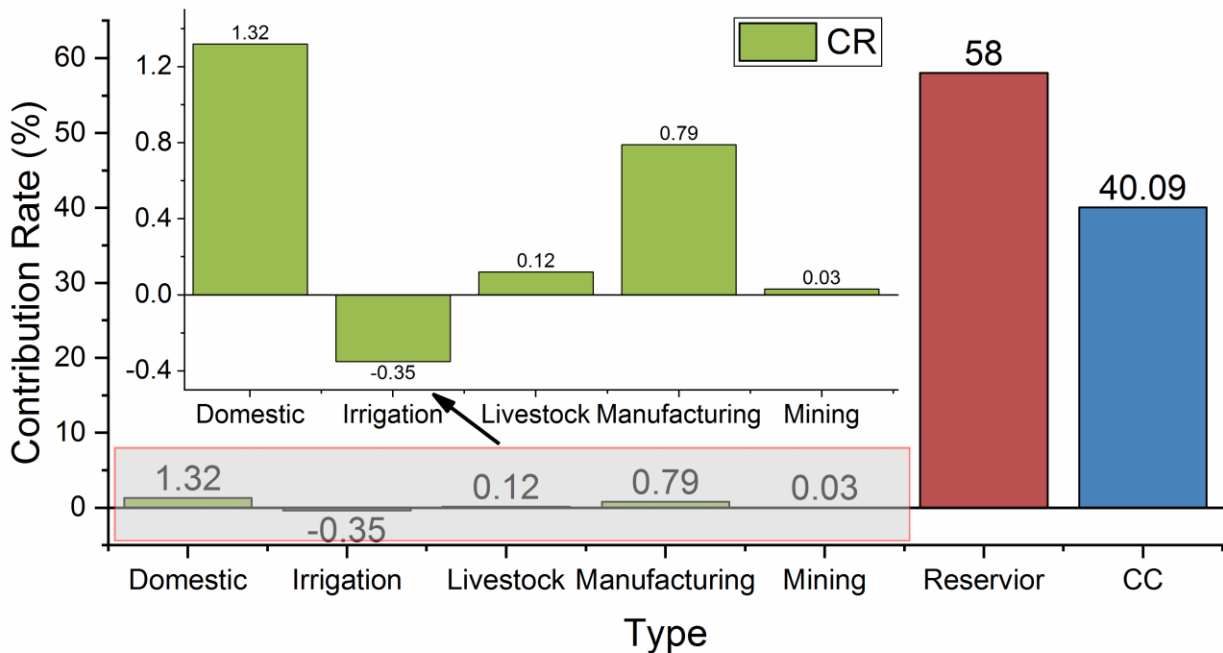
Fig. 14. Contribution rate (CR) of Domestic, Irrigation, Livestock, Manufacturing, and Mining water withdrawals and reservoir construction and climate change (CC) to the streamflow changes at Yunjinghong station from 1970 to 2010.

5. Discussion

5.1 How does parameter uncertainty affect the quantitative results?

In this paper, we proposed a novel framework to quantify the CR of CC and HAs to streamflow changes considering the
uncertainty of hydrological simulations. This is because the phenomenon of "equifinality for different parameters" in hydrological
simulations greatly affects the quantification results. To preliminarily investigate the impact of model simulation uncertainty of
the quantitative results, we selected the two simulation results with the largest NSEs in this study for analysis. The evaluation
metrics and CR of CC and HAs are shown in Table 7, which shows that both simulations can simulate the monthly streamflow at
Yunjinghong station in the LR Basin accurately, and the two simulations have almost the same evaluation performance. However,
the attribution analysis obtained from the two hydrological simulations showed completely different results. In the first simulation
result, according to the method introduced in Section 3.4.1, the streamflow changes in the LR Basin were mainly caused by CC,
but in the second hydrological simulation, the opposite conclusion was drawn, that is, HAs dominated. These were almost the
same hydrological simulation results but with opposite conclusions from the attribution analysis; this was one of the reasons why
we must consider the uncertainty of the model parameters in the attribution analysis of CC and HAs using hydrological simulations.
The results of Section 4.3.1 and related published studies (Han et al., 2019) in the LR Basin show that the streamflow changes in
the LR Basin were mainly caused by HAs.

Table 7 Results of the CR of climate change and human activities to runoff changes with almost equal model performance
(monthly) using the SWAT model

Simulation	Calibration		Validation		Overall		Contribution Rate (%)	
result	NSE	RE (%)	NSE	RE (%)	NSE	RE (%)	CC	HA
1st simulation	0.94	-10.6	0.95	-8.6	0.94	-9.97	54.5	45.5
2nd simulation	0.94	-7.7	0.95	-8.7	0.94	-8.1	42.1	57.9

(Notation: CC and HA represent the climate change and human activities, respectively; NSE and RE represent the Nash-
Sutcliffe efficiency coefficient and the relative error, respectively)

Table 8 shows the values of 9 highly sensitive parameters of the two simulation results and the streamflow values simulated by
the two simulations in the natural period and the impacted period. Table 8 and the calculation methods introduced in Section 3.4.1
show that the watershed streamflow reduction caused by CC calculated by the 1st and 2nd simulation results was -217.1 m^3/s and
-170.6 m^3/s, respectively, which was the reason why they had opposing calculated attribution results. From the perspective of
specific parameter values, the most sensitive parameter is ALPHA_BNK, which was the base flow alpha factor for bank storage
(days) characterized by the bank storage recession curve. The difference between the two calibration results was not large, and
this parameter mainly controlled the baseflow process, having little effect on the average annual streamflow while the difference
in CH_K2 in the two calibration results was larger, at 303.87 and 106.12. This parameter represented the effective hydraulic
conductivity of the main channel alluvial layer, which meant that the larger the CH_K2 value is, the more likely the water in the
main channel is lost to groundwater; accordingly, the streamflow production at the outlet of the watershed would decrease (Arnold
et al., 2012b; Xu et al., 2016; Zhao et al., 2018a). This might also be one of the reasons that the first simulated streamflow (1617
m^3/s) was slightly smaller than the second one (1667.9 m^3/s). The SFTMP parameter, which was the temperature when
precipitation was converted into snowfall, returned values for the first simulation and the second simulation as 2.69°C and -0.11°C,
respectively; this meant that in the first simulation, more liquid precipitation was converted into a solid state and less streamflow

625 was formed, which also led to a smaller simulated streamflow in the first simulation. The SMTMP parameter, which was the snow melt base temperature, was -4.13°C in the first simulation result and 3.73°C in the second simulation result. From basic physical knowledge, the SMTMP parameter in the second calibration result was more reasonable. Compared with other research results with similar terrain features in this study area, Debele et al. (2010) constructed the SWAT model in the high altitude area of the source of the Yellow River, China, and the SMTMP value obtained was 4°C. The difference between the two simulations was not

630 large for the set of the other parameters (SOL_BD, GW_REVAP, CN2 and SOL_K), or the parameter that controlled the baseflow (ALPHA_BF) had little effect on the average streamflow of the basin. Based on the above, the second simulation results were consistent with the calculation results of the new framework proposed in this study. Therefore, when we choose a hydrological simulation to analyze the attribution of CC and HAs to streamflow variations, we should clearly also consider the actual physical meaning and the uncertainties of the model parameters.

635 **Table 8** Values of 9 sensitivity parameters with similar simulation results and their simulated streamflow in the natural and impacted periods

Simulation No.	1st simulation	2nd simulation
V__ALPHA_BNK	0.84	0.68
V__CH_K2	303.87	106.12
V__SOL_BD	1.51	1.93
V__GW_REVAP	0.03	0.003
V__SFTMP	2.69	-0.11
R__CN2	-0.06	-0.12
R__SOL_K	0.32	0.31
V__SMTMP	-4.13	3.73
V__ALPHA_BF	0.11	0.77
Simulated streamflow in the NP (m^3/s)	1617.6	1667.9
Simulated streamflow in the IP (m^3/s)	1400.5	1497.3

(Notation: NP = "Natural period", IP = "Impacted period", R_, V_, and A_ represent multiplying, replacing, and adding the corresponding parameter values, respectively, in the process of calibrating the parameters.)

In this study, 575 parameter combinations with good simulation results (NSE greater than 0.75) were selected, with a step size

640 of 5%, it is proposed to reduce the influence of hydrological modeling uncertainty on the quantitative results by constructing the posterior histogram distribution of the CR of CC and HAs to watershed streamflow change. However, it is undeniable that there are still unreasonable parameter combinations in the simulation results with high probability (167 times). For the LR basin, it is almost impossible to obtain the measured values of all 9 parameters with high sensitivity (Table 3). Therefore, in order to further explore the possible influence of unreasonable parameter values on the quantitative results, we selected two parameters related to

645 snowmelt streamflow (SMTMP and SFTMP) to exclude unreasonable parameter combinations. According to the parameter value ranges recommended by Abbaspour et al. (2007) and other related references (Arnold et al., 2012a; Yang et al., 2017), in this study, the reasonable value range of these two parameters is set to -5 to 5 °C. After excluding parameter combinations outside this value range, we obtained 55 simulation results with relatively reasonable parameter values, and the quantization results obtained from this calculation are shown in Fig. 15. It can be seen from Fig. 15 that after excluding unreasonable parameter combinations,

650 the calculated CR of CC in the LR Basin to the reduction of streamflow is 45-50% (with an average CR of 47.1%), and this result

is consistent with the results presented in Fig. 10 which derived from the novel framework proposed in our study. At the same time, it is also proved that although the calculation framework proposed in this study may contain unreasonable parameter combinations in obtaining the simulation results with the highest frequency, the calculation results are still highly accurate. In addition, for the research area where the measured values of related parameters can be obtained, the rationality and authenticity of the parameter values should be fully considered while selecting the parameter combination with higher NSE.
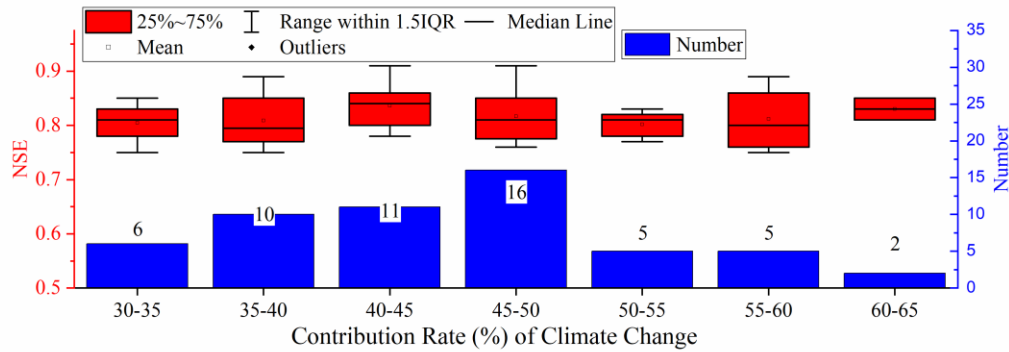
Fig. 15 Histogram of the number of simulations of the CR (with 5% steps) of climate change to streamflow reduction in the LR Basin at the annual scale and corresponding Nash-Sutcliffe Efficiency box plots after excluding the parameter combinations.

5.2 Land use/land cover change in the LR Basin from 1980 to 2015

In Section 4.4, the water withdrawals of domestic, irrigation, mining, livestock, and manufacturing, and in addition, dead storage capacity of constructed reservoirs as well as the impact of HAs were separated; then the impacts of HAs on streamflow changes were separated. However, HAs also influenced the land use change on rainfall-runoff characteristics. Fig. 16 shows the land use in the LR Basin in1980, 2000, 2010 and 2015. Farmland was the largest land use in the upper LR Basin, while the lower reaches were dominated by forest. Due to the high-altitude terrain in the upper reaches, unused land and glaciers were mainly distributed in this area. Table 9 shows the areas of land use types in the LR Basin in 1980, 1990, 2000, 2010 and 2015. In general, the water area of the LR Basin showed a significant reduction from 1980 to 1990, which was possibly due to the decrease in the area of glaciers due to the increase in temperature from 1980 to 1990 (Fig. 6). In contrast, the water area increased by nearly 30% from 2010 to 2015, which was mainly due to the construction of Nuozhadu hydropower station (with a total storage capacity of 22.7 km^3) within the basin.

Table 9 Areas (km^2) of land use types in the LR Basin in 1980, 1990, 2000, 2010 and 2015

Land use type	1980	1990	2000	2010	2015
Farmland	6978	6978	7034	6954	6888
Forest	33381	33633	33342	33417	33304
Grassland	42547	42652	42511	42500	42430
Water	944	593	615	615	825
City	87	112	113	129	164
Unused land	5515	5865	5837	5837	5841
Permanent glacier	724.6	206.7	247.5	247.5	243.1

(Nation: Permanent glacier in Table 5 is second-level type which belong to Water)

The area of farmland in the LR Basin showed a decreasing trend during 2000-2010 and 2010-2015, which is also the main reason for the reduction in the irrigation water consumption in the basin, which is consistent with the results shown in Fig. 13.

The areas of the cities all showed an increasing trend in the three periods of 1980-2000, 2000-2010 and 2010-2015 (by 29.8%,

675   14.1% and 27.1%, respectively), while the other three types of land use/land cover (i.e., forest, grassland, and unused land) did

not change significantly in the three periods. In summary, no significant changes were found from 1980 to 2015 in the forest and

grassland of the LR Basin (accounting for 37.3% and 47.5% of the total area, respectively). Although the city area has undergone

significant changes, it accounts for a very small total area of the basin very (0.09%). The change in the water area was mainly due

to the construction of the reservoirs, so the method used in Section 4.3 to separate the contribution of HAs to the reduction in the

680   streamflow in the LR Basin used is reasonable.
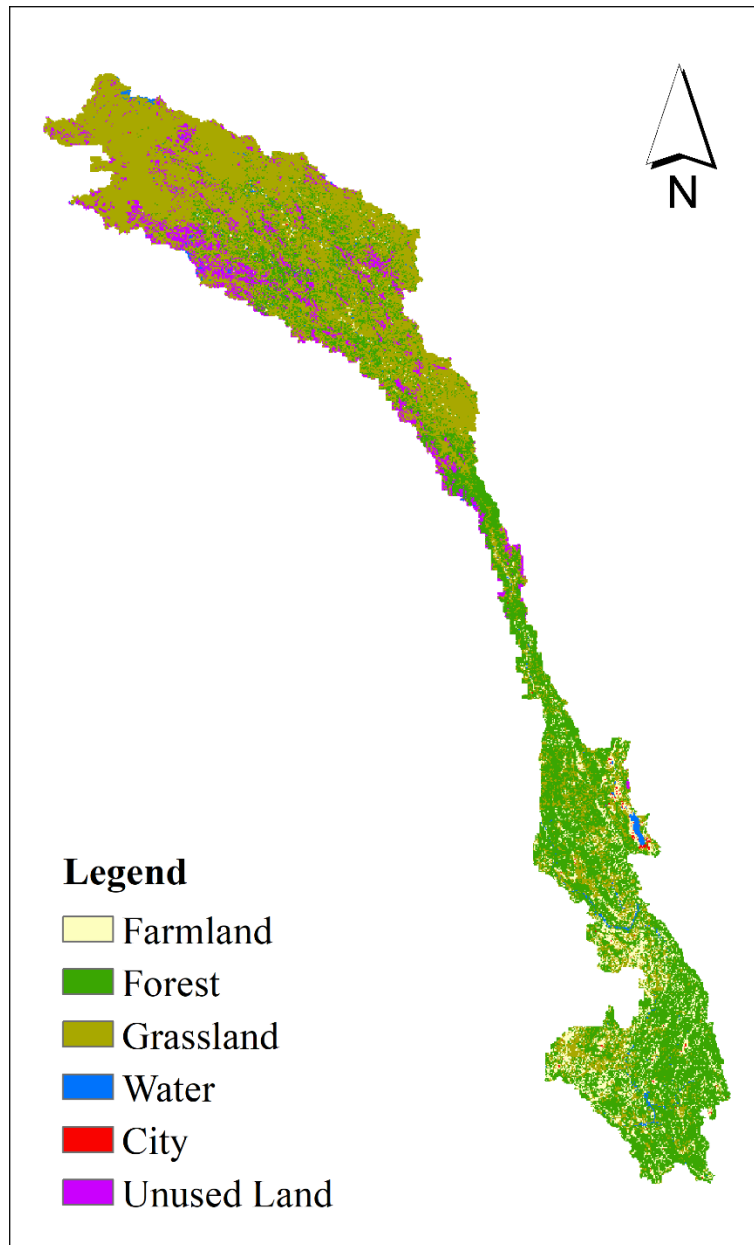
Fig. 16. Land use classification in the LR Basin in 2015.

5.3 Comparison with results of other published studies

685   As analyzed above, there was no particularly significant change in the precipitation and potential evapotranspiration from 1961 to 2015 in the LR Basin. HAs mainly included the construction of reservoirs, resulting in changes in the streamflow. Attribution analysis results showed that the CR of HAs was 57.6%, and the corresponding CC was 42.4%. This result was basically consistent with Han et al. (2019), but the CR of HAs was smaller than the results of Han et al. research results (95%). This may be due to the following reasons:

690   1) The streamflow data of different time spans were used to obtain different break points. They used streamflow data from 1980 to 2014 to obtain the break point in 2008, and this study used data from 1961 to 2015 to identify the break point in 2005.

     2) Different hydrological models were used. They used the coupled routing and excess storage (CREST) model with an NSE of 0.57, while the SWAT model used in this study had an NSE of 0.94.

     3) Longer series of streamflow data and simulation data were used.

695   As indicated by Li et al. (2017a) and (Han et al., 2019), as the streamflow data series became longer in the impacted period, the impact of reservoir scheduling on the streamflow changes on an average scale for many years gradually decreased. Li et al. (2017a) selected Chiang Saen station, which was the nearest station to Yunjinghong station downstream of the LR Basin, for their research, and then they divided the streamflow series into three stages, the pre-impact period (1960-1991), the transition period (1992-2009) and the post-impact period (2010-2014). They concluded that the construction of the reservoirs in the LR Basin led

700   to a decrease in the streamflow process during the flood period and an increase in the dry period, which was consistent with the results of our study (Section 4.3.2). Their results also showed that HAs contributed 61.88% to the streamflow reduction at Chiang Saen station, which was also close to the results of our study (57.4%).

5.4 Applicability and uncertainty of the proposed framework

     A new quantitative framework for calculating the CR of CC and HAs to watershed streamflow variations was proposed in this

705   study, and it was successfully applied to the LR Basin with relatively accurate results. From our perspective, this method can effectively quantify the influence of the "equifinality for different parameters" that may exist in the use of hydrological simulation methods to quantify the CR of CC and HAs. At the same time, we also believe that this framework can be applied to other watersheds based on the following aspects. First, in the section 4.4, the Budyko framework and sectional water withdrawal data within the basin were used to compare with the new framework. Second, the results of the comparison with published research on

710   the LR Basin (Han et al., 2019) also proved that the framework has good accuracy and applicability. Third, in the process of comparing with the new framework, we fully considered the impact of various HAs within the study area, including five types of water withdrawals (i.e., irrigation, livestock, living, mining, and manufacturing), the impact of reservoir storage and the land use/land cover change. Of course, due to the highly nonlinear relationship between the parameters of the hydrological model, we suggest that readers ensure that the selected simulation results with NSEs greater than 0.75 are large enough when applying the

715   novel framework in other research areas (this study had 500 simulations). It is undeniable that this method still has certain uncertainties and limitations when it is applied to other watersheds. First, if there are multiple break points in the annual streamflow sequence, then when selecting the unique break point, it is necessary to consider the abrupt change points of the time series of other meteorological elements (precipitation, temperature, etc.) in the basin. At the same time, the impact of strong human activities (reservoir construction, large-scale water transfer project construction, etc.) on the abrupt change of streamflow in the

720   basin should also be considered (Dey and Mishra, 2017). Finally, a unique break point is selected to divide the research time series

into a natural period and an impacted period, and then the quantitative framework proposed in this study can be applied. Second, because the SWAT model has good applicability at the Yunjinghong station in the LR Basin, it can meet the 500 best simulation requirements set by the framework proposed in this study, but the hydrological model may have different applicability in different research areas. Therefore, the application of this framework in other research areas may have limitations, which need to be further verified. Third, because this study uses the parameter combinations obtained by the natural period to input the meteorological element data of the impacted period for calculation, this may also bring uncertainty to the calculation results, which is usually called "transferability" (Fu et al., 2018).

Although the new quantitative framework proposed in this study considers the uncertainties in hydrological simulations, the framework is still based on traditional hydrological simulation methods to separate the CR of CC to streamflow change, and then to deduce the CR of HAs. Therefore, inevitably, there are still uncertainties in the calculation process. For example, the construction of large-scale reservoirs and changes in land use/land cover (urbanization, etc.) are important factors that alter the climatic state of a local region, specifically in that they change the temporal and spatial distribution characteristics of local regional hydrometeorological elements (Li et al., 2017c; Degu et al., 2011). This change in meteorological elements was regarded as part of the impact of CC in this study; however, it was also caused by both HAs (reservoir construction) and CC. On the other hand, there are uncertainties in the division of the natural period and the impacted period in this study, which assumed that the impact of HAs on streamflow changes in the natural period was negligible; however, there were almost no periods within a watershed that were completely unaffected by HAs, and the impact of HAs on streamflow variations in the natural period was ignored in these studies. In this study, there was also strong disturbance of HAs during the natural period (i.e., reservoir construction: Manwan and Dachaoshan) (Table 1). In addition, our study selected the NSE as the objective function to calibrate the SWAT model, which may also bring uncertainties in the quantitative results. As indicated by (Gupta et al., 2009) and Gupta and Kling (2011), using the NSE as an objective function to calibrate a hydrological model may tend to underestimate the peak streamflow. Although the CR in our study was calculated by the average streamflow over multiple years, it still brought a given amount of uncertainty to the quantitative results. Therefore, follow-up research should strengthen the optimization of the objective function and benefit from field investigation of the actual meaning of the parameters. Since the impacts of CC and HAs on the hydrological processes of the watershed are complicated and interconnected, it is still a challenge to completely separate the impacts of CC and HAs on streamflow variations (Xin et al., 2019). Further consideration should be given to quantify the impact of specific HAs, such as land use change and water withdrawal, and then to separate the impact of CC and HAs on streamflow changes as completely as possible.

6. Conclusions

In this study, we proposed a new framework that considered the uncertainties of model simulations to quantify the CR of CC and HAs to streamflow changes. This framework was developed based on the posterior histogram frequency distribution (PHD) of the CR of CC and HAs. Then, we selected the LR Basin for the case study. Over the past three decades, after the construction of the Manwan Reservoir in 1987, six large reservoirs were constructed within the basin before 2014. The streamflow process in the watershed also has significant changes on multiyear average and monthly scales. The Mann-Kendall monotonic trend test and the Mann-Kendall break point test were used to test the trend and identify the break point of the annual streamflow data at Yunjinghong station within the period of 1961 to 2015. Then, the available period was divided into the natural period (before the

break point) and the impacted period (after the break point). Afterwards, the SWAT model and the SUFI-2 method were used to construct the Posterior Histogram Distribution (PHD) of the CR of CC and HAs. Finally, the Budyko framework and the basin wide gridded monthly sectoral water use (GMSWU) data set were used to compare with the newly proposed framework. The main conclusions of this study are as follows:

1) The new proposed framework can be used to quantify the CR of CC and HAs in the LR Basin which can fully solve the local optimal solution for hydrological simulation parameters in current related studies. The results of comparison using the Budyko framework and Gridded Monthly Sectoral Water Use (GMSWU) data set also showed that the new framework has high accuracy (the error range is within 6%).

2) The break point of the streamflow sequence during 1961-2015 at Yunjinghong station was identified in 2005. The streamflow significantly decreased (~ -22%) after 2005 compared with that of the natural period (1961 - 2004), which was mainly due to the construction of the Xiaowan Reservoir in October 2004. Significantly reduced streamflow in the flood period and significantly increased streamflow during the dry period also occurred, which was mainly due to the capacity adjustment of the constructed reservoirs. The trend test results also showed that from 1961 to 2015, the annual streamflow in the LR Basin showed a significant decreasing trend at the $\alpha = 0.01$ significance level, precipitation showed a nonsignificant decreasing trend, and mean temperature showed a significant increasing trend at the $\alpha = 0.01$ significance level.

3) The quantification results calculated using the new proposed framework showed that, on an annual scale, compared with the natural period of 1961 – 2004, the CR of CC and HAs (CR of CC and HAs) were 40 - 45% (with an average CR of 42.6%) and 55 – 60% (with an average CR of 57.4%), respectively. The CR of CC and HAs derived from the Budyko framework were 37.2% and 62.8%, respectively, and the error between the two calculation results was 5.4%. The CR of HAs calculated using the GMSWU data and the reservoirs dead capacities was 58.0%, which also proved that the new proposed framework in this study can be used in the LR Basin.

4) Quantitative analysis results on a monthly scale in the LR Basin showed that, except for June and November, streamflow changes in other months were caused by HAs. Further analysis showed that the streamflow in June during the impacted period decreased by 6.9 mm compared with that in the natural period, while the precipitation and potential evapotranspiration decreased and increased by 20.2 mm and 8.83 mm, respectively; the streamflow decreased by 5.34 mm in November, while the corresponding precipitation and potential evapotranspiration changed by -7.43 mm and 5.52 mm, respectively.

In summary, this study provides a new calculation framework that considers the uncertainty of hydrological simulations to quantify the CR of CC and HAs to streamflow changes. The results of this case study also provide a reference for understanding the dominant factors of streamflow changes in the LR Basin and improving water resource management measures for the transboundary Lancang-Mekong River Basin. Of course, this new proposed framework also needs to be applied and verified in more research areas. In addition, this framework only considers the dual impacts of CC and HAs. However, in practical applications, water resource decision makers are more willing to understand the specific impacts of HAs such as irrigation water and land use changes. Therefore, in future research, efforts should be made to expand the framework to quantify the CRs of individual items of CC and HAs.

Acronyms:

AE – Actual Evaporation; CC – Climate Change; CGDPA – China Gauge-based Daily Precipitation Analysis; CMA – China Meteorological Administration; CR – Contribution Rate; CREST - Coupled Routing and Excess Storage; DEM - Digital Elevation Model; GMSWU - Global gridded Monthly Sectoral Water Use data set; HA – Human Activity; HRU – Hydrologic Response Unit; HWSD V1.2 – Harmonized World Soil Database Version 1.2; LR – Lancang River; NSE – Nash-Sutcliffe Efficiency coefficient; PET - Potential Evapotranspiration; PHD - Posterior Histogram Distribution; RE – Relative Error; SRTM - Shuttle Radar Topography Mission; SUFI -2: Sequential Uncertainty Fitting Procedure version 2; SWAT – Soil & Water Assessment Tool; USDA - US Department of Agriculture Research Service.

Author contributions

Xiongpeng Tang Proposed the research framework and wrote the draft manuscript. Guobin Fu and Chao Gao Improved the language of the manuscript. Guoqing Wang provided the data for this study. Cuishan Liu, Yanli Liu, Zhenxin Bao, Silong Zhang and Junliang Jin Jointly processed the data, helped build the hydrological model.

Competing interests

The authors declare that they have no conflict of interest.

Code and data availability

The observed streamflow data from the Information Center of the Ministry of Water Resources and the local water resources management department are available upon request from the corresponding author (gqwang@nhri.cn) and the first author (xptanghhu@163.com). The observed precipitation, temperature, wind speed, relative humidity data sets can be downloaded from https://data.cma.cn/.

Acknowledgements

This research was financially sponsored by two research programs in China: (1) the National Key Research and Development Program (No. 2018YFC1508104), (2) the National Natural Science Foundation of China (No. 92047301,52079079,51879163), and, (3) the Second Tibetan Plateau Scientific Expedition and Research Program (No. 2019QZKK0203).

References:

Abbaspour, K. C., Johnson, C. A., and Genuchten, M. T. V.: Estimating Uncertain Flow and Transport Parameters Using a Sequential Uncertainty Fitting Procedure, Vadose Zone Journal, 3, 1340-1352, 10.2113/3.4.1340, 2004.
Abbaspour, K. C., Genuchten, M. T. V., Schulin, R., and Schläppi, E.: A sequential uncertainty domain inverse procedure for estimating subsurface flow and transport parameters, Water Resources Research, 33, 1879-1892, 10.1029/97WR01230, 1997.

820   Abbaspour, K. C., Yang, J., Maximov, I., Siber, R., Bogner, K., Mieleitner, J., Zobrist, J., and Srinivasan, R.: Modelling hydrology and water quality in the pre-alpine/alpine Thur watershed using SWAT, J Hydrol, 333, 413-430, 10.1016/j.jhydrol.2006.09.014, 2007.

Arnold, J. G., Srinivasan, R., Muttiah, R. S., and Williams, J. R.: Large area hydrologic modeling and assessment part I: model development, JAWRA Journal of the American Water Resources Association, 34, 73-89, 10.1111/j.1752-
825   1688.1998.tb05961.x, 1998.

Arnold, J. G., Kiniry, J. R., Srinivasan, R., Williams, J. R., Haney, E. B., and Neitsch, S. L.: Soil & Water Assessment Tool: Input/Output Documentation. Version 2012, Texas Water Resources Institute, College Station, 1-650 pp.2012a.

Arnold, J. G., Moriasi, D. N., Gassman, P. W., Abbaspour, K. C., White, M. J., Srinivasan, R., Santhi, C., Harmel, R., Van Griensven, A., and Van Liew, M. W.: SWAT: Model use, calibration, and validation, Transactions of the ASABE,
830   55, 1491-1508, 10.13031/2013.42246, 2012b.

Bao, Z. X., Zhang, J. Y., Wang, G. Q., Fu, G. B., He, R. M., Yan, X. L., Jin, J. L., Liu, Y. L., and Zhang, A. J.: Attribution for decreasing streamflow of the Haihe River basin, northern China: Climate variability or human activities?, J Hydrol, 460, 117-129, 10.1016/j.jhydrol.2012.06.054, 2012.

Beven, K.: A manifesto for the equifinality thesis, J Hydrol, 320, 18-36, 10.1016/j.jhydrol.2005.07.007, 2006.
835   Beven, K. and Binley, A.: The future of distributed models: model calibration and uncertainty prediction, Hydrological processes, 6, 279-298, 10.1002/hyp.3360060305, 1992.

Budyko, M. I.: The heat balance of the earth's surface, Soviet Geography, 2, 3-13, 10.1080/00385417.1961.10770761, 1961.

Chandesris, A., Looy, K. V., Diamond, J. S., and Souchon, Y.: Small dams alter thermal regimes of downstream water,
840   Hydrol Earth Syst Sc, 23, 4509-4525, 10.5194/hess-23-4509-2019, 2019.

Debele, B., Srinivasan, R., and Gosain, A.: Comparison of process-based and temperature-index snowmelt modeling in SWAT, Water Resour Manag, 24, 1065-1088, 10.1007/s11269-009-9486-2, 2010.

Degu, A. M., Hossain, F., Niyogi, D., Pielke Sr, R., Shepherd, J. M., Voisin, N., and Chronis, T.: The influence of large dams on surrounding climate and precipitation patterns, Geophysical Research Letters, 38,
845   10.1029/2010GL046482, 2011.

Dey, P. and Mishra, A.: Separating the impacts of climate change and human activities on streamflow: A review of methodologies and critical assumptions, J Hydrol, 548, 278-290, 10.1016/j.jhydrol.2017.03.014, 2017.

Farsi, N. and Mahjouri, N.: Evaluating the contribution of the climate change and human activities to runoff change under uncertainty, J Hydrol, 574, 872-891, 10.1016/j.jhydrol.2019.04.028, 2019.
850   Fu, G., Chen, S., Liu, C., and Shepard, D.: Hydro-climatic trends of the Yellow River basin for the last 50 years, Climatic Change, 65, 149-178, 10.1023/B:CLIM.0000037491.95395.bb, 2004.

Fu, G., Charles, S. P., Chiew, F. H., Ekström, M., and Potter, N. J.: Uncertainties of statistical downscaling from predictor selection: Equifinality and transferability, Atmospheric research, 203, 130-140, 10.1016/j.atmosres.2017.12.008, 2018.
855   Gao, C., Liu, L., Ma, D., He, K., and Xu, Y.-P.: Assessing responses of hydrological processes to climate change over the southeastern Tibetan Plateau based on resampling of future climate scenarios, Science of the Total Environment, 664, 737-752, 10.1016/j.scitotenv.2019.02.013, 2019.

Gilbert, R. O.: Statistical methods for environmental pollution monitoring, John Wiley & Sons1987.

Grumbine, R. E. and Xu, J.: Mekong Hydropower Development, Science, 332, 178-179, 10.1126/science.1200990,
860   2011.

Gupta, H. V. and Kling, H.: On typical range, sensitivity, and normalization of Mean Squared Error and Nash-Sutcliffe Efficiency type metrics, Water Resources Research, 47, 10.1029/2011WR010962, 2011.

Gupta, H. V., Kling, H., Yilmaz, K. K., and Martinez, G. F.: Decomposition of the mean squared error and NSE performance criteria: Implications for improving hydrological modelling, J Hydrol, 377, 80-91,
865   10.1016/j.jhydrol.2009.08.003, 2009.

Hamed, K. H. and Ramachandra Rao, A.: A modified Mann-Kendall trend test for autocorrelated data, J Hydrol, 204, 182-196, 10.1016/S0022-1694(97)00125-X, 1998.

Han, Z., Long, D., Fang, Y., Hou, A., and Hong, Y.: Impacts of climate change and human activities on the flow regime of the dammed Lancang River in Southwest China, J Hydrol, 570, 96-105, 10.1016/j.jhydrol.2018.12.048,
870   2019.

Hegerl, G., Black, E., Allan, R., Ingram, W., Polson, D., Trenberth, K., Chadwick, R., Arkin, P., Sarojini, B., and Becker, A.: Challenges in quantifying changes in the global water cycle, Bulletin of the American Meteorological Society, 100, 1097-1115, 10.1175/BAMS-D-13-00212.1, 2015.

Hennig, T., Wang, W., Feng, Y., Ou, X., and He, D.: Review of Yunnan's hydropower development. Comparing small and large hydropower projects regarding their environmental implications and socio-economic consequences, Renewable and Sustainable Energy Reviews, 27, 585-595, 10.1016/j.rser.2013.07.023, 2013.

Huang, Z., Hejazi, M., Li, X., Tang, Q., Vernon, C., Leng, G., Liu, Y., Döll, P., Eisner, S., Gerten, D., Hanasaki, N., and Wada, Y.: Reconstruction of global gridded monthly sectoral water withdrawals for 1971–2010 and analysis of their spatiotemporal patterns, Hydrol. Earth Syst. Sci., 22, 2117-2133, 10.5194/hess-22-2117-2018, 2018.

Jacobs, J. W.: The Mekong River Commission: Transboundary Water Resources Planning and Regional Security, Geographical Journal, 168, 354-364, 10.1111/j.0016-7398.2002.00061.x 2002.

Kendall, M.: Rank correlation methods (4th edn.) charles griffin, San Francisco, CA, 8, 1975.

Kong, D., Miao, C., Wu, J., and Duan, Q.: Impact assessment of climate change and human activities on net runoff in the Yellow River Basin from 1951 to 2012, Ecological Engineering, 91, 566-573, 10.1016/j.ecoleng.2016.02.023, 2016.

Lee, S., Yeo, I. Y., Sadeghi, A. M., Mccarty, G. W., Hively, W. D., Lang, M. W., and Sharifi, A.: Comparative analyses of hydrological responses of two adjacent watersheds to climate variability and change using the SWAT model, Hydrology & Earth System Sciences, 22, 689-708, 10.5194/hess-22-689-2018, 2018.

Li, D., Long, D., Zhao, J., Lu, H., and Hong, Y.: Observed changes in flow regimes in the Mekong River basin, J Hydrol, 551, 217-232, 10.1016/j.jhydrol.2017.05.061, 2017a.

Li, L. J., Zhang, L., Wang, H., Wang, J., Yang, J. W., Jiang, D. J., Li, J. Y., and Qin, D. Y.: Assessing the impact of climate variability and human activities on streamflow from the Wuding River basin in China, Hydrological Processes: An International Journal, 21, 3485-3491, 10.1002/hyp.6485, 2007.

Li, Y., Li, Z., Dai, M., and Wei, L.: Effect evaluation of emergency water supplement from cascade reservoirs on Lancang River to Mekong River in 2016, Yangtze River (in Chinese), 48, 56-60, 2017b.

Li, Y., Zhou, W., Chen, X., Fang, D., and Zhang, Q.: Influences of the Three Gorges Dam in China on precipitation over surrounding regions, Journal of Meteorological Research, 31, 767-773, 10.1007/s13351-017-6177-4, 2017c.

Liang, K., Liu, C., Liu, X., and Song, X.: Impacts of climate variability and human activity on streamflow decrease in a sediment concentrated region in the Middle Yellow River, Stochastic environmental research and risk assessment, 27, 1741-1749, 2013.

Liu, J., Zhang, Q., Singh, V. P., and Shi, P.: Contribution of multiple climatic variables and human activities to streamflow changes across China, J Hydrol, 545, 145-162, 10.1016/j.jhydrol.2016.12.016, 2017.

Liu, J., Zhou, Z., Yan, Z., Gong, J., Jia, Y., Xu, C.-Y., and Wang, H.: A new approach to separating the impacts of climate change and multiple human activities on water cycle processes based on a distributed hydrological model, J Hydrol, 578, 124096, 10.1016/j.jhydrol.2019.124096, 2019.

Liu, Q. and Liang, L.: Impacts of climate change on the water balance of a large nonhumid natural basin in China, Theoretical and applied climatology, 121, 489-497, 10.1007/s00704-014-1255-3, 2015.

Malagò, A., Pagliero, L., Bouraoui, F., and Franchini, M.: Comparing calibrated parameter sets of the SWAT model for the Scandinavian and Iberian peninsulas, Hydrological Sciences Journal, 60, 949-967, 10.1080/02626667.2014.978332, 2015.

Mann, H. B.: Nonparametric tests against trend, Econometrica: Journal of the Econometric Society, 245-259, 10.2307/1907187, 1945.

Moriasi, D. N., Arnold, J. G., Van Liew, M. W., Bingner, R. L., Harmel, R. D., and Veith, T. L.: Model evaluation guidelines for systematic quantification of accuracy in watershed simulations, Transactions of the ASABE, 50, 885-900, 10.13031/2013.23153, 2007.

Nash, J. E. and Sutcliffe, J. V.: River flow forecasting through conceptual models part I—A discussion of principles, J Hydrol, 10, 282-290, 10.1016/0022-1694(70)90255-6, 1970.

Piman, T., Cochrane, T., and Arias, M.: Effect of proposed large dams on water flows and hydropower production in the Sekong, Sesan and Srepok rivers of the Mekong Basin, River research and applications, 32, 2095-2108, 10.1002/rra.3045, 2016.

Piman, T., Cochrane, T., Arias, M., Green, A., and Dat, N.: Assessment of flow changes from hydropower development and operations in Sekong, Sesan, and Srepok rivers of the Mekong basin, Journal of Water Resources Planning and Management, 139, 723-732, 10.1061/(ASCE)WR.1943-5452.0000286, 2012.

Shen, Y., Zhao, P., Pan, Y., and Yu, J.: A high spatiotemporal gauge-satellite merged precipitation analysis over China, Journal of Geophysical Research: Atmospheres, 119, 3063-3075, 10.1002/2013JD020686, 2014.

Sneyers, R.: On the statistical analysis of series of observations, 1431991.

Song, X., Zhang, J., Zou, X., Zhang, C., AghaKouchak, A., and Kong, F.: Changes in precipitation extremes in the Beijing metropolitan area during 1960–2012, Atmospheric Research, 222, 134-153, 10.1016/j.atmosres.2019.02.006, 2019.

Tang, G., Long, D., Hong, Y., Gao, J., and Wan, W.: Documentation of multifactorial relationships between precipitation and topography of the Tibetan Plateau using spaceborne precipitation radars, Remote Sensing of Environment, 208, 82-96, 10.1016/j.rse.2018.02.007, 2018.

Tang, X., Zhang, J., Wang, G., Yang, Q., Yang, Y., Guan, T., Liu, C., Jin, J., Liu, Y., and Bao, Z.: Evaluating Suitability of Multiple Precipitation Products for the Lancang River Basin, Chinese Geographical Science, 29, 37-57, 10.1007/s11769-019-1015-5, 2019.

Teuling, A. J., De Badts, E. A., Jansen, F. A., Fuchs, R., Buitink, J., Van Dijke, A. J. H., and Sterling, S. M.: Climate change, reforestation/afforestation, and urbanization impacts on evapotranspiration and streamflow in Europe, Hydrol Earth Syst Sc, 23, 3631-3652, 10.5194/hess-23-3631-2019, 2019.

Tilt, B. and Gerkey, D.: Dams and population displacement on China's Upper Mekong River: Implications for social capital and social–ecological resilience, Global Environmental Change, 36, 153-162, 10.1016/j.gloenvcha.2015.11.008, 2016.

Tuo, Y., Duan, Z., Disse, M., and Chiogna, G.: Evaluation of precipitation input for SWAT modeling in Alpine catchment: A case study in the Adige river basin (Italy), Science of the Total Environment, 573, 66-82, 10.1016/j.scitotenv.2016.08.034, 2016.

Wang, G. Q., Zhang, J. Y., Pagano, T. C., Liu, Y. L., Liu, C. S., Bao, Z. X., Jin, J. L., and He, R. M.: Using hydrological simulation to detect human-disturbed epoch in runoff series, Water Sci Technol, 71, 691-699, 10.2166/wst.2014.526, 2015.

Wang, W., Shao, Q., Yang, T., Peng, S., Xing, W., Sun, F., and Luo, Y.: Quantitative assessment of the impact of climate variability and human activities on runoff changes: a case study in four catchments of the Haihe River basin, China, Hydrological Processes, 27, 1158-1174, 10.1002/hyp.9299, 2013.

Wu, H. and Chen, B.: Evaluating uncertainty estimates in distributed hydrological modeling for the Wenjing River watershed in China by GLUE, SUFI-2, and ParaSol methods, Ecological Engineering, 76, 110-121, 10.1016/j.ecoleng.2014.05.014, 2015.

Xie, J., Xu, Y.-P., Wang, Y., Gu, H., Wang, F., and Pan, S.: Influences of climatic variability and human activities on terrestrial water storage variations across the Yellow River basin in the recent decade, J Hydrol, 579, 124218, 10.1016/j.jhydrol.2019.124218, 2019.

Xie, P., Yatagai, A., Chen, M., Hayasaka, T., Fukushima, Y., Liu, C., and Yang, S.: A Gauge-Based Analysis of Daily Precipitation over East Asia, Journal of Hydrometeorology, 8, 607-626, 10.1175/JHM583.1, 2007.

Xin, Z., Li, Y., Zhang, L., Ding, W., Ye, L., Wu, J., and Zhang, C.: Quantifying the relative contribution of climate and human impacts on seasonal streamflow, J Hydrol, 574, 936-945, 10.1016/j.jhydrol.2019.04.095, 2019.

Xu, H., Xu, C. Y., Chen, S., and Chen, H.: Similarity and difference of Global reanalysis datasets (WFD and APHRODITE) in driving lumped and distributed hydrological models in a humid region of China, J Hydrol, 542, 343-356, 10.1016/j.jhydrol.2016.09.011, 2016.

Xu, M., Kang, S., Wu, H., and Yuan, X.: Detection of spatio-temporal variability of air temperature and precipitation based on long-term meteorological station observations over Tianshan Mountains, Central Asia, Atmospheric Research, 203, 141-163, 10.1016/j.atmosres.2017.12.007, 2018.

Xue, Z., Liu, J. P., and Ge, Q.: Changes in hydrology and sediment delivery of the Mekong River in the last 50 years: connection to damming, monsoon, and ENSO, Earth Surface Processes & Landforms, 36, 296-308, 10.1002/esp.2036, 2011.

Yang, J., Reichert, P., Abbaspour, K. C., Xia, J., and Yang, H.: Comparing uncertainty analysis techniques for a SWAT application to the Chaohe Basin in China, J Hydrol, 358, 1-23, 10.1016/j.jhydrol.2008.05.012, 2008.

Yang, L., Feng, Q., Yin, Z., Wen, X., Si, J., Li, C., and Deo, R. C.: Identifying separate impacts of climate and land use/cover change on hydrological processes in upper stream of Heihe River, Northwest China, Hydrological Processes, 31, 1100-1112, 10.1002/hyp.11098, 2017.

975 Zhang, L., Dawes, W., and Walker, G.: Response of mean annual evapotranspiration to vegetation changes at catchment scale, Water resources research, 37, 701-708, 10.1029/2000WR900325, 2001.

Zhao, F., Wu, Y., Qiu, L., Sun, Y., Sun, L., Li, Q., Niu, J., and Wang, G.: Parameter uncertainty analysis of the SWAT model in a mountain-loess transitional watershed on the Chinese Loess Plateau, Water-Sui, 10, 690, 10.3390/w10060690, 2018a.

980 Zhao, F., Wu, Y., Qiu, L., Sivakumar, B., Zhang, F., Sun, Y., Sun, L., Li, Q., and Voinov, A.: Spatiotemporal features of the hydro-biogeochemical cycles in a typical loess gully watershed, Ecological Indicators, 91, 542-554, 10.1016/j.ecolind.2018.04.027, 2018b.

Zhao, Q., Liu, S., Deng, L., Dong, S., Yang, J., and Wang, C.: The effects of dam construction and precipitation variability on hydrologic alteration in the Lancang River Basin of southwest China, Stochastic Environmental
985 Research & Risk Assessment, 26, 993-1011, 10.1007/s00477-012-0583-z, 2012.